Available online at www.sciencedirect.com
SCIENCE DIRECT
Hearing Research 214 (2006) 45–67
Hearing Research
www.elsevier.com/locate/heares

Research paper

Fast cochlear amplification with slow outer hair cells

Timothy K. Lu [a,b], Serhii Zhak [a], Peter Dallos [c], Rahul Sarpeshkar [a,*]

[a] *Analog VLSI and Biological Systems Group, Research Lab of Electronics, Massachusetts Institute of Technology, 77 Massachusetts Avenue, Room 38-276, Cambridge, MA 02139, USA*
[b] *Harvard-MIT Division of Health Sciences and Technology, 77 Massachusetts Avenue, Room E25-219, Cambridge, MA 02139, USA*
[c] *Auditory Physiology Laboratory, Departments of Neurobiology and Physiology and Communication Sciences and Disorders, Northwestern University, Evanston, IL 60208, USA*

Received 2 November 2005; received in revised form 25 January 2006; accepted 27 January 2006

Abstract

In mammalian cochleas, outer hair cells (OHCs) produce mechanical amplification over the entire audio-frequency range (up to 100 kHz). Under the 'somatic electromotility' theory, mechano-electrical transduction modulates the OHC transmembrane potential, driving an OHC mechanical response which generates cycle-by-cycle mechanical amplification. Yet, though the OHC *motor* responds up to at least 70 kHz, the OHC membrane RC time constant (in vitro upper limit ~1000 Hz) reduces the potential driving the motor at high frequencies. Thus, the mechanism for high-frequency amplification with slow OHCs has been a two-decade-long mystery. Previous models fit to experimental data incorporated slow OHCs but did not explain how the OHC time constant limitation is overcome. Our key contribution is showing that negative feedback due to organ-of-Corti functional anatomy with adequate OHC gain significantly extends closed-loop system bandwidth and increases resonant gain. The OHC gain-bandwidth product, not just bandwidth, determines if high-frequency amplification is possible. Due to the cochlea's collective traveling-wave architecture, a single OHC's gain need not be great. OHC piezoelectricity increases the effectiveness of negative-feedback but is not essential for amplification. Thus, emergent closed-loop network dynamics differ significantly from open-loop component dynamics, a generally important principle in complex biological systems.

Keywords: Cochlear amplifier; Outer hair cell; Receptor potential; Membrane time constant low-pass filtering; Electromotility; Negative feedback

1. Introduction

According to the somatic electromotility theory, cochlear amplification is driven by mechano-electrical transduction which changes the OHC membrane potential to cause mechanical OHC contraction and extension, which in turn generates amplification of sound (Brownell et al., 1985; Neely and Kim, 1986). However, the OHC membrane RC time constant has an in vitro upper limit of ~1000 Hz (Housley and Ashmore, 1992; Preyer et al., 1996) while the OHC motor can operate up to at least 70 kHz (Frank et al., 1999). As a result, the membrane RC time constant is expected to reduce the transmembrane potential driving the OHC motor at high frequencies and therefore, the mechanism by which high-frequency amplification takes places in mammalian cochleas is unclear (Santos-Sacchi, 2003). To explain how amplification up to 100 kHz can be achieved by slow OHCs, a whole host of theories have been proposed, none of which, however, has gained wide acceptance (Santos-Sacchi, 2003; Mountain and Hubbard, 1994; Dallos and Evans, 1995; Nobili and Mammano, 1996; Ospeck et al., 2003; Spector et al., 2003; Weitzel et al., 2003; Spector, 2005; Spector et al.,

Abbreviations: OHC, outer hair cell; RC, resistance-capacitance or resistor-capacitor; DC, direct current; TM, tectorial membrane; RL, reticular lamina; CF, characteristic frequency; BM, basilar membrane; IHC, inner hair cell

* Corresponding author. Tel.: +1 617 253 4872; fax: +1 617 253 5210.
E-mail address: rahuls@mit.edu (R. Sarpeshkar).

0378-5955/$ - see front matter © 2006 Elsevier B.V. All rights reserved.
doi:10.1016/j.heares.2006.01.018

2005). An alternative proposed mechanism for cochlear amplification is oscillatory hair-bundle motion, which may be important in non-mammalian vertebrates, which lack OHCs (Choe et al., 1998). Active force generation by OHC stereocilia may also be present in mammals and would not be limited by the slow OHC time constant (Chan and Hudspeth, 2005; Kennedy et al., 2005). However, somatic OHC motility has been shown to underlie mammalian amplification (Liberman et al., 2002; Cheatham et al., 2004). Previous models that incorporated the OHC time constant were able to match some experimental data, but did not explain the mechanism by which the time constant limitation was surpassed (Geisler and Sang, 1995; Fukazawa, 1997; Neely, 1993; Dimitriadis and Chadwick, 1999). Our theory for fast cochlear amplification by negative feedback via somatic electromotility does not require novel mechanisms and results from an engineering analysis of cochlear mechanics. The theory we describe here is not mutually exclusive with the theory that viscous forces from the organ of Corti provide some compensation for the OHC time constant and may be complementary (Nobili and Mammano, 1996; Scherer and Gummer, 2004a; Gummer et al., 1996). Furthermore, our theory does not exclude active force generation by mammalian OHC stereocilia but instead demonstrates how somatic electromotility may overcome the OHC time constant limitation. Though we present a simplified model of cochlear mechanics to illustrate our major insights, the model can also be extended to incorporate higher-order mechanical dimensionality and non-linearity to further improve congruence with experiments.

Negative feedback rather than positive feedback is often utilized in engineering to alter closed-loop system dynamics and to counteract attenuation due to slow time constants. A feedback loop is said to have negative feedback if the loop's corrective action opposes the effect of the input at DC (which stands for direct current, meaning at a frequency of 0 Hz) and to have positive feedback if the loop's action aids the effect of the input at DC. At non-DC frequencies, dynamics in the loop will alter the phase of the corrective action with respect to the input, but by definition, the sign at DC determines the sign of the feedback. Open-loop systems with high gain and low bandwidth can be transformed into closed-loop systems with lower gain and higher bandwidth by using negative feedback. Thus, the key figure of merit is the gain-bandwidth product, and the ability of a system to operate at high frequencies in negative-feedback topologies is not limited by the open-loop bandwidth. Negative feedback in cochlear function has been proposed first by Mountain et al. (1983) although we emphasize the role of negative feedback in OHC speedup and they proposed negative feedback around the basilar membrane whereas we use negative feedback around the reticular lamina. A portion of this work was announced at the Ninth International Mechanics of Hearing Workshop held in Portland, Oregon in July, 2005 (Lu et al., in press).

1.1. Basic feedback analysis

Any negative-feedback loop can be analyzed in a block diagram by decomposing the system into a scalar gain, a block that models the dynamics of the feed-forward system, and a block that models the feedback dynamics (Fig. 1). The frequency characteristics of each block are represented using Laplace transforms in the s-plane ($s = j\omega$ where $j = \sqrt{-1}$ and $\omega = 2\pi f$) (Bode, 1945). Black's formula captures all the dynamics of the closed-loop feedback system, where the loop gain is defined as $|KA(s)B(s)|$ and the loop transmission is $-KA(s)B(s)$ since the sign of the feedback is negative:

$$\frac{Y(s)}{X(s)} = \frac{KA(s)}{1 + KA(s)B(s)} \tag{1}$$

The roots of the denominator in the s-plane are referred to as the poles of the system and the roots of the numerator are referred to as the zeros of the system. The poles of the system describe the inherent dynamics of the system response and are independent of which input–output transfer function is computed. The zeros of the system change depending on which input–output transfer function is computed.

As evident from Eq. (1), the closed-loop dynamics will be equal to the open-loop dynamics when there is no feedback ($B(s) = 0$) but will increasingly deviate from the open-loop dynamics as K increases with a non-zero $B(s)$. High loop gains also often drive the closed-loop system unstable. Negative feedback gives the system designer the ability to construct closed-loop systems that have significantly different dynamics from the constituent parts. Negative feedback is often used in electromechanical systems to increase the gain of resonant systems and extend low-frequency bandwidths (Franklin et al., 2002).

Operational amplifiers (op-amps) are commonly used devices in electronics. Op-amps usually come with high gains but very low bandwidths. When used with negative feedback, however, gain can be traded for bandwidth. For example, in unity negative feedback, where the output is directly fed back into the input as in Fig. 2, operational amplifiers can be transformed from high gain ($A = 10^6$) and low bandwidth (1 Hz) to low gain (1) and high band-

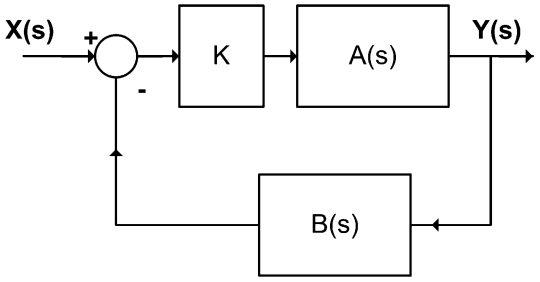

Fig. 1. Block diagram of negative feedback with a scalar gain K, feed-forward dynamics captured by $A(s)$, and feed-back dynamics captured by $B(s)$. $X(s)$ is the input into the system and $Y(s)$ is the output.

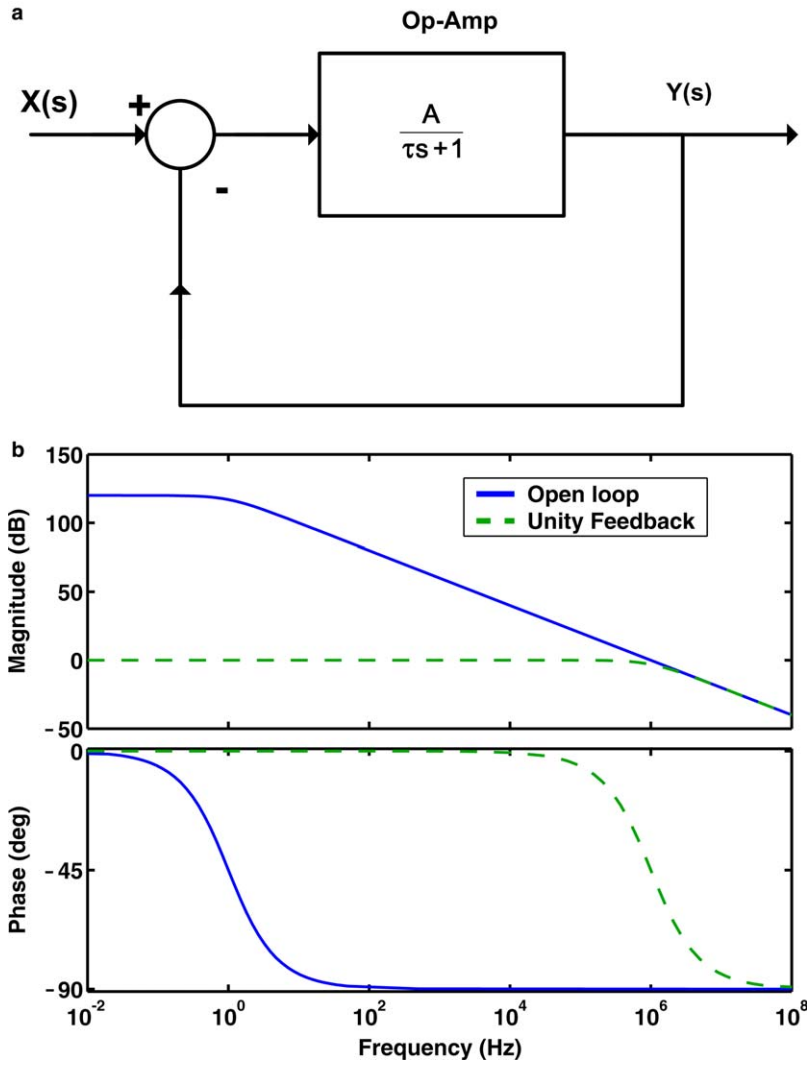

Fig. 2. A high-gain, low-bandwidth operational amplifier is converted into a low-gain, high-bandwidth amplifier via unity negative feedback where the output is directly fed back into the input. (a) Block diagram of the unity-feedback configuration shows that the output is directly hooked up into the input via negative feedback. The gain is A and the time constant for the amplifier is τ. (b) Magnitude and phase plots show that the open-loop characteristic of the operational amplifier (*solid line*, *blue*) has high gain (10^6) but low bandwidth (1 Hz). In the unity feedback configuration (*dashed line*, *green*), the system has low gain (1) but high bandwidth (10^6 Hz). (For interpretation of the references in colour in this figure legend, the reader is referred to the web version of this article.)

width (10^6 Hz). In both cases, the gain-bandwidth product is constant at 10^6 Hz.

In tachometer feedback, slow motor time constants are sped up by sensing the motor velocity via a tachometer and feeding this signal back into the input that is driving the motor (Fig. 3a). As shown in Fig. 3b, increasing the tachometer gain decreases the DC magnitude of the output but increases the bandwidth. In this configuration, the closed-loop transfer function, $Y(s)/X(s)$, is equal to $[1/(\tau \times s + 1)]/[1 + K/(\tau \times s + 1)] = [1/(1 + K)]/[\tau_{cl} \times s + 1]$, where $\tau_{cl} = \tau/(1 + K)$. Therefore, in this configuration, the closed-loop time constant, τ_{cl}, is a factor $(1 + K)$ less than the open-loop time constant, τ. Negative feedback with gain results in faster system dynamics because the active component generates a large input drive that brings the output to the desired level more quickly.

Thus, it is difficult to draw conclusions about the behavior of a closed-loop system (such as the in vivo characteristics of the cochlea) simply by taking open-loop measurements of the individual components (such as the OHC bandwidth in vitro).

Our inspiration for how the cochlea may perform amplification despite the OHC time constant limitation came from the analysis of a simple engineering-based system (Fig. 4a). When one wishes to amplify the output of a "plant" system, i.e. the resonant block in Fig. 4a, the simplest method is to use an amplifier. However, all real-world amplifiers have an inherent frequency limitation most commonly modeled by a single slow time constant. Luckily, if these amplifiers have extra gain, then one can trade DC gain for bandwidth to allow high-frequency operation by using negative feedback. An example of such a system is shown

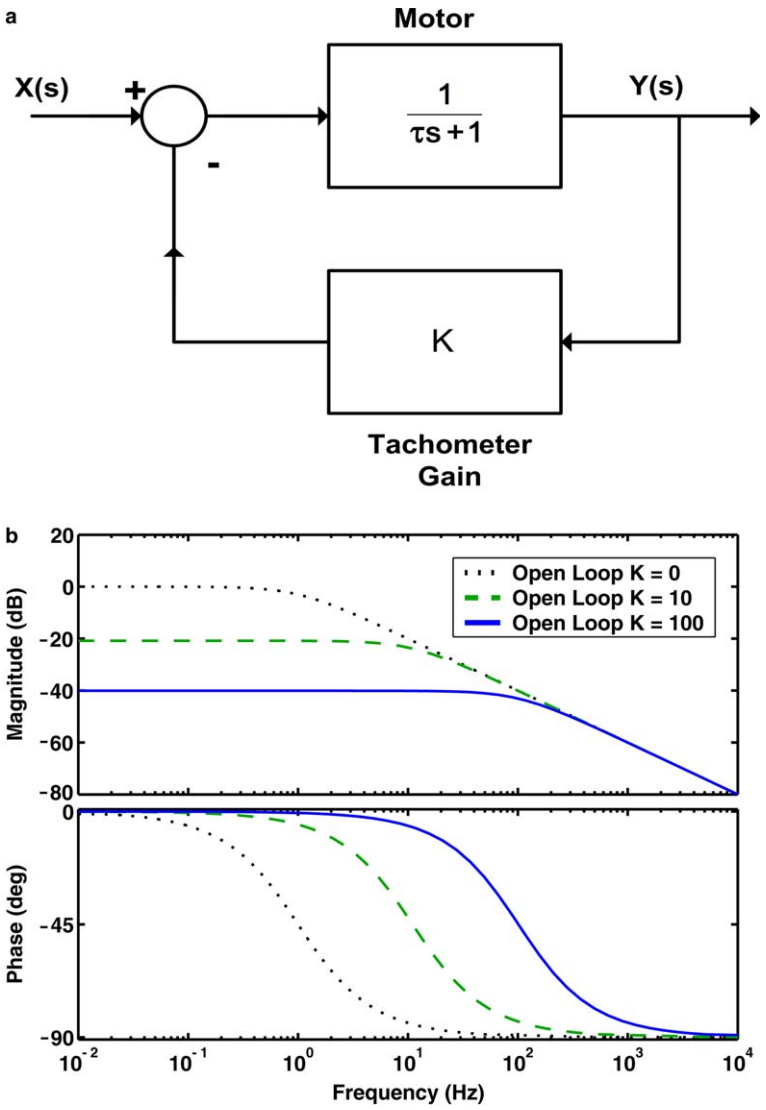

Fig. 3. A slow motor with time constant τ can be sped up with tachometer feedback where the output velocity of the motor is sensed by a tachometer with gain K which feeds back into the input with negative feedback. (a) Block diagram of the tachometer feedback configuration shows that the slow motor is in the forward path and the tachometer is in the feedback path. (b) The motor has low bandwidth in the open-loop configuration (*dotted line*, *black*). By increasing the tachometer gain, K, the DC magnitude is reduced but the bandwidth is increased (*dashed line*, *green* and *solid line*, *blue*). (For interpretation of the references in colour in this figure legend, the reader is referred to the web version of this article.)

in Fig. 4a, where the amplifier is characterized by gain, K_{ohc}, and a time constant, τ_{ohc}. If one were to use the amplifier with the resonant block in an open-loop configuration (Fig. 4b), the DC magnitude would be high but an early rolloff due to the amplifier time constant and a low amount of resonant gain due to the low quality factor of the resonant block would limit high frequency operation. If used in negative feedback (Fig. 4b), however, the DC magnitude is reduced but in return, the amplifier time constant does not affect the output until higher frequencies while the resonant gain near the resonant frequency of the resonant block is increased. As a result, high frequency operation is possible and the output magnitude is especially increased at the resonant frequency. We believe that this simple example captures the essence of what allows high-frequency amplification in the cochlea despite the OHC membrane time constant. The actual details of the biological system are slightly more complicated and are described below.

2. Materials and methods

2.1. Micromechanical model

To gain insight into the effect of negative feedback on cochlear mechanics, we first looked at a local section of the cochlea at the basal end, where the OHC time constant is most limiting to high-frequency amplification.

Since the tectorial membrane–reticular lamina (TM–RL) complex and basilar membrane (BM) have been characterized as separate resonant subsystems (Zwislocki and Kletsky, 1979; Allen, 1980; Mammano and Ashmore, 1993; Gummer et al., 1996), we adopt a model with two resona-

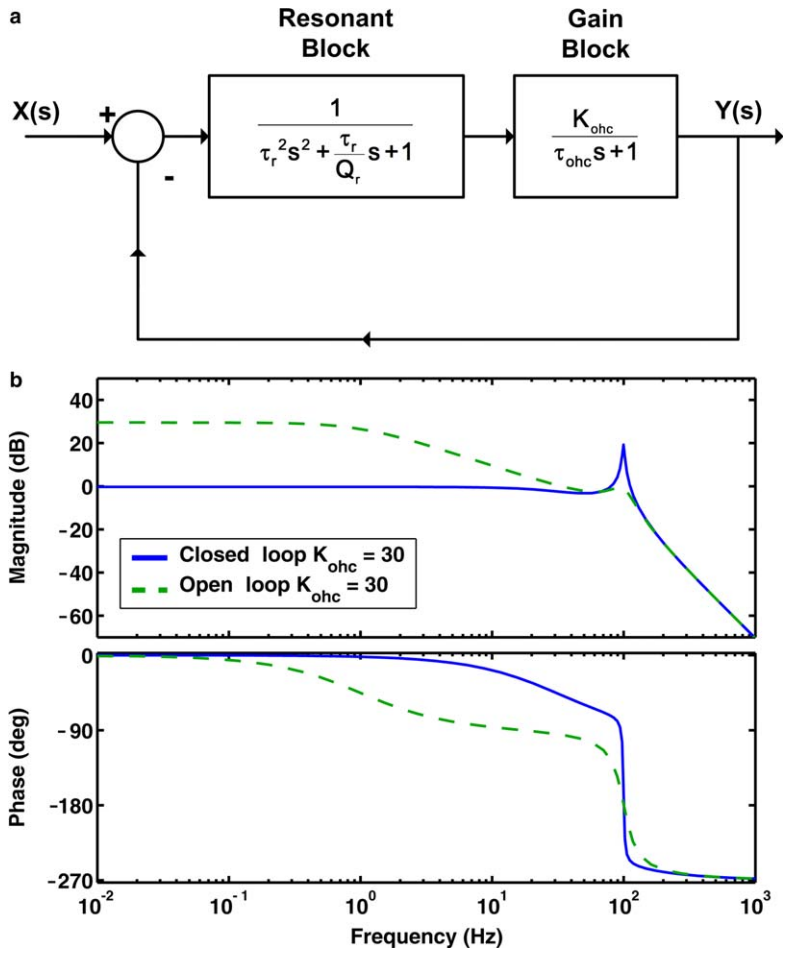

Fig. 4. A second-order resonant block and a gain block with a time constant τ_{ohc} and gain K_{ohc} connected in negative feedback can be used to increase resonant gain and decrease the effective closed-loop time constant. (a) Block diagram of the feedback configuration shows that the resonant gain block and gain block are in the forward path. (b) The magnitude of the open-loop output (*dashed line*, *green* with $K_{ohc} = 30$) has a high DC value but begins to roll off early due to the gain block time constant. The closed-loop configuration (*solid line*, *blue* with $K_{ohc} = 30$) has a lower DC magnitude, but begins to roll off later and has a higher resonant gain. The reduction of the time constant rolloff effect on the output and increased resonant gain due to negative feedback is the essence of what allows amplification in spite of the OHC time constant in the cochlea. (For interpretation of the references in colour in this figure legend, the reader is referred to the web version of this article.)

tors coupled together by the OHC passive somatic stiffness and the OHC force generator (Fig. 5) (Markin and Hudspeth, 1995). Fig. 5a and b show the OHC feedback mechanism present in the cochlea's organ of Corti. An upward motion of the basilar membrane due to an acoustic input causes radial reticular lamina (RL) shear towards the modiolus related to upwards RL motion, an opening of stereocilia ion channels, depolarization of the OHC membrane, and consequent contractile forces exerted by the OHC on the BM and RL. The contractile force on the RL has a corrective action on the stereocilia motion that rotates the stereocilia towards the modiolus, thus reducing OHC membrane potential and opposing the action of the input. Hence, we have negative feedback. The contractile force on the BM appears to cause positive feedback, but in this topology, the RL corrective action always dominates over the BM corrective action. More formally, as shown below, the *return ratio* of the OHC force generator, a useful concept defined in Bode (1945) for studying the feedback effects of a circuit element, is dependent only on RL motion, and is therefore always negative at DC.

The two resonator model is shown in Fig. 5c where R refers to damping, k refers to stiffness, M refers to mass, F refers to force, and X to displacement (see Table 1 for specific variable definitions). We did not explicitly model the TM but instead lumped it into the TM-RL complex because TM and RL motion are coupled (see Section 3). Therefore, from here on, whenever we refer to the RL, we implicitly mean the TM-RL complex as a whole, and we shall use this simplification through most of the paper. Because OHC shortening and lengthening in situ is accompanied by RL shear away from and towards the modiolus, respectively, we did not explicitly represent radial RL movement in the model. Instead, we assumed that radial RL movement away from the modiolus was kinematically coupled to upwards RL motion and vice versa, lumping both motions into one effective velocity variable (U_{rl}) (Reuter and Zenner, 1990). Thus, in our

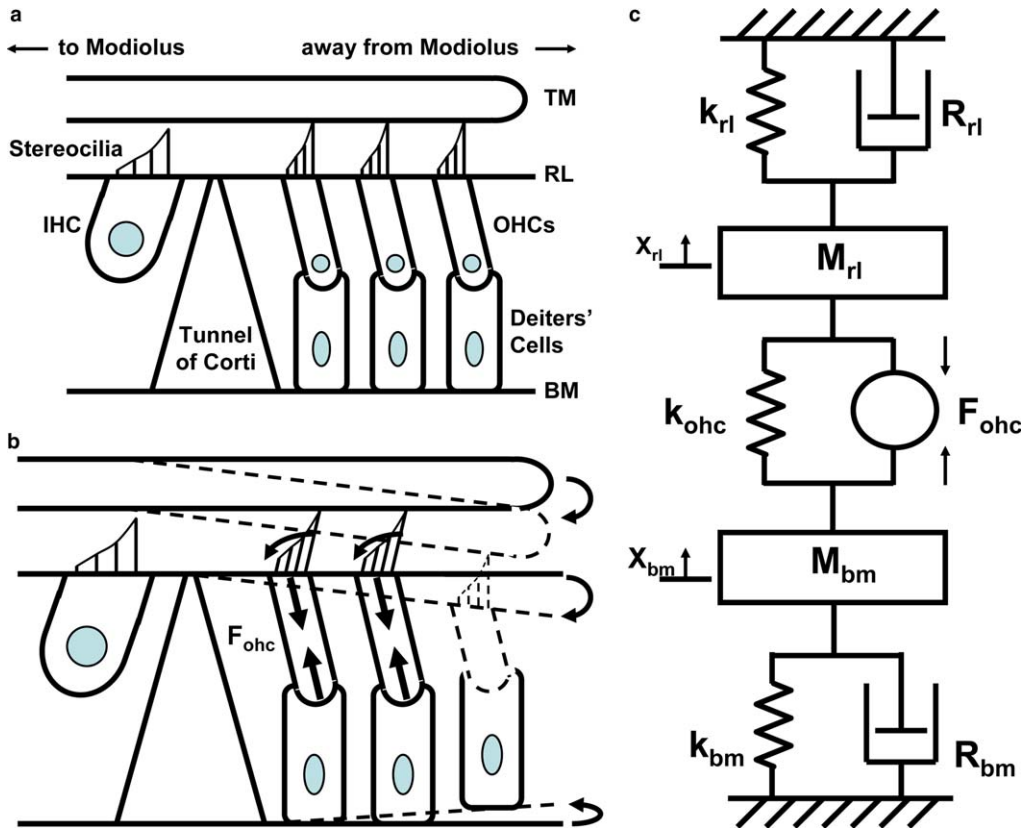

Fig. 5. Organ-of-Corti micromechanical model (not to scale). (a) OHCs are between the RL and the BM. OHC stereocilia tips are embedded in the TM while IHC stereocilia are not. Abbreviation not in text – Inner Hair Cells (IHCs). (b) OHC depolarization moves stereocilia towards the modiolus leading to negative feedback (see text). Note that the rightmost OHC drawn in dotted lines shows how a shortened OHC brings its stereocilia to a more upright position. (c) Organ-of-Corti mechanical representation. The TM-RL complex and BM are represented by resonant subsystems (Zwislocki and Kletsky, 1979; Allen, 1980) coupled together by an OHC stiffness and the somatic electromotility force generator, F_{ohc}, defined as positive for contraction due to membrane potential depolarization.

model, RL displacement determines stereocilia displacement and so the force generated by OHCs, F_{ohc}, is proportional to the RL displacement, X_{rl}, or equivalently to the integrated RL velocity, U_{rl}/s. We define the DC RL-displacement-to-voltage ratio as k_v, the DC OHC voltage-to-force gain as k_f, and the OHC time constant as τ (see Section 2.3 for parameter derivations). The OHC force generator is then given by:

$$F_{ohc} = \frac{k_f \times k_v \times X_{rl}}{\tau s + 1} = \frac{k_f \times k_v \times U_{rl}}{s \times (\tau s + 1)} \quad (2)$$

Note that F_{ohc} is positive for contraction and $s = j\omega$ where $j = \sqrt{-1}$ and $\omega = 2\pi f$. Active OHC stiffness can be added to this model to account for the voltage-dependent stiffness but is not necessary for the basic insights described here (Deo and Grosh, 2004). Since our interest is threshold phenomena at low signal levels, where BM motion and cochlear potentials asymptote to linear behavior, we model our system linearly. Non-linearity can be included in the model if desired.

The respective mechanical impedances in Fig. 6 are Z_{rl}, Z_{bm}, and Z_{ohc} and are derived from Fig. 5c. The OHC force generator is represented in Eq. (2) using s-plane notation as having a low-pass characteristic.

$$Z_{bm} = \frac{1}{sC_{bm}} + R_{bm} + sM_{bm} \quad (3)$$

$$Z_{rl} = \frac{1}{sC_{rl}} + R_{rl} + sM_{rl} \quad (4)$$

$$Z_{ohc} = \frac{1}{sC_{ohc}} \quad (5)$$

The mechanical admittances, Y_{bm}, Y_{rl}, and Y_{ohc}, are the inverses of the respective mechanical impedances. The membrane voltage is v_m in Fig. 6.

Based on the micromechanical model, we derive a block diagram demonstrating the negative-feedback loop in this system (Fig. 6). We split up the total net force borne by the RL, F_{rl} (where $F_{rl} \equiv Z_{rl} \times U_{rl}$), into a component due to the active OHC, $F_{rl,ohc}$, and a component due to forces from any other external source, $F_{rl,ext}$ (Fig. 6). These forces are defined as positive upwards. $F_{rl,ext}$ may be composed of multiple forces, i.e., any force on the RL coupled from the BM by the OHC stiffness, any force due to pressure within the organ of Corti, or any force on the RL from fluid pressure in the scalae. Only a fraction of the OHC force generator, F_{ohc}, is applied to the RL as $F_{rl,ohc}$ (Fig. 6).

The return ratio, a useful concept defined in Bode (1945) for studying the feedback effects of a circuit element such as

Table 1
Parameters used for micromechanical and macromechanical simulations were derived from experimental data reported in the literature

Name	Meaning	Value	Units
x	Position along the cochlea	–	cm
L	Length of cochlea[a]	1.85	cm
CF	Characteristic frequency[a]	$350 \cdot \left(10^{2.1\cdot\frac{L-x}{L}} - 0.85\right)$	Hz
H_{ohc}	OHC length[b]	$32.4324 \cdot x + 20$	μm
H_{cilia}	OHC stereocilia height[c]	$2.4865 \cdot x + 1.2$	μm
$C_{bm} = k_{bm}^{-1}$	BM compliance (with 25 μm probe)[d]	$0.182 \cdot e^{3.464\cdot x}$	m/N
$C_{rl} = k_{rl}^{-1}$	RL compliance (with 25 μm probe)[e]	$6 \cdot C_{bm}$	m/N
$L_{bm} = M_{bm}$	BM mass	$\frac{1}{(2\pi\cdot CF)^2\cdot C_{bm}}$	kg
$L_{rl} = M_{rl}$	RL mass	$0.2 \cdot M_{bm}$	kg
Q_{bm}	BM quality factor	$6 \cdot e^{-2.303\cdot\frac{x}{L}}$	–
Q_{rl}	RL quality factor	$4 \cdot e^{-2.303\cdot\frac{x}{L}}$	–
R_{bm}	BM damping	$\frac{1}{Q_{bm}}\left(\frac{M_{bm}}{C_{bm}}\right)^{0.5}$	N · s/m
R_{rl}	RL damping	$\frac{1}{Q_{rl}}\left(\frac{M_{rl}}{C_{rl}}\right)^{0.5}$	N · s/m
$C_{ohc} = k_{ohc}^{-1}$	Single OHC compliance[f]	$2.7778 \cdot H_{ohc}$	m/N
k_v	Single OHC DC RL-displacement-to-voltage ratio[g]	4	mV/nm
k_f	Single OHC voltage-to-force gain[h]	$0.5 \cdot (e^{-2.7\cdot x} - 0.00035)$	nN/mV
G_K	OHC basolateral conductance[b]	$-0.6503 \cdot H_{ohc} + 55.7$	nS
C_m	OHC basolateral membrane capacitance[b]	$0.3574 \cdot H_{ohc} + 5.8416$	pF
τ	OHC membrane time constant[b]	$\frac{C_m}{G_K}$	ms

A total of 1028 sections were used, corresponding to a length of 18 μm per section or two OHC diameters. References are included where relevant.
[a] Greenwood (1990).
[b] Housley and Ashmore (1992).
[c] Wright (1984).
[d] Emadi et al. (2004).
[e] Mammano and Ashmore (1993).
[f] He and Dallos (1999).
[g] Housley and Ashmore (1992), He et al. (2004), Ospeck et al. (2003).
[h] Frank et al. (1999), Mountain and Hubbard (1994), Dong et al. (2002), Iwasa and Chadwick (1992), Scherer and Gummer (2004b).

an active generator, is the loop transmission in our model. The loop transmission is given by the multiplicative product around the loop in Fig. 6 and includes the negative sign of the feedback:

$$-\frac{k_f k_v}{s(\tau s+1)}\frac{Z_{bm}}{Z_{rl}Z_{bm}+Z_{rl}Z_{ohc}+Z_{bm}Z_{ohc}} = -\frac{k_f k_v}{s(\tau s+1)}\frac{Y_{ohc}Y_{rl}}{Y_{bm}+Y_{rl}+Y_{ohc}} \quad (6)$$

Because all of the parameters are positive at DC, the loop transmission or return ratio of the active OHC generator is always negative at DC. Therefore, we have negative feedback regardless of parameter magnitudes. The loop gain is the absolute value of the loop transmission. Since the RL stiffness is less than the BM stiffness (Mammano and Ashmore, 1993), the loop gain is higher than it would be if the BM stiffness were made smaller, implying that the cochlea's intrinsic parameters help to maximize negative feedback.

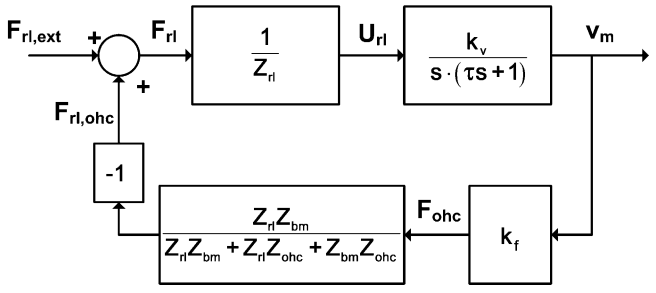

Fig. 6. Block diagram demonstrating the negative feedback loop (see text for variable definitions). Negative feedback in the micromechanical model speeds up the effective closed-loop OHC membrane time constant.

Note that the loop gain is approximately proportional to the OHC gain (k_f) multiplied by the OHC bandwidth ($1/\tau$) for frequencies much greater than the OHC bandwidth ($\tau s \gg 1$) so that at the characteristic frequency (CF), which is much greater than the OHC bandwidth at the basal end, it is the OHC gain-bandwidth product and not the gain or bandwidth alone that determines the loop gain and thus the effectiveness of the feedback. Of course, passive parameters such as Y_{ohc}, Y_{rl}, and Y_{bm} play important roles in determining the strength of the loop gain as well. Based on Eq. (6), parameter values that reduce Y_{bm} (such as increasing BM stiffness) or parameters that increase Y_{ohc} (such as increasing OHC compliance at a fixed k_f) or Y_{rl} (such as increasing RL compliance) will increase the loop gain.

We have neglected fluid coupling in computing the return ratio (Eq. (6)) in our micromechanical model. This is clearly a simplification and may be an issue worth considering in future work. It is theoretically possible to compute this return ratio if the characteristic impedance of the

tapered lines, present in the macromechanical cochlea, to the right and left of the given micromechanical section can be analytically computed and used to create lumped impedances in the micromechanics. However, for the macromechanical model described in the section below, such calculations are not simple, and we have not incorporated them in this work.

Analysis of the micromechanical model was performed using Matlab® 6.5.

2.2. Macromechanical model

Since the micromechanical model demonstrated the importance of negative feedback in permitting adequate OHC force at resonance and reducing the effect of the membrane RC circuit, we constructed a macromechanical model to show that our model with negative feedback and slow outer hair cells was able to produce realistic simulation of experimental data.

We used a discrete-element traveling-wave transmission-line sandwich model for the macromechanical simulation of the cochlea (de Boer, 1990a,b; Hubbard et al., 2000). The model consists of micromechanical sections coupled together by fluid through the scala vestibuli and media, the organ-of-Corti, and the scala tympani with parameters scaled from base to apex (Fig. 7). To incorporate the parameters described below, we divided the entire length of the cochlea into 1028 micromechanical sections, each corresponding to a length of 18 μm, which is consistent with the 21 μm longitudinal space constant observed for the BM (Emadi et al., 2004). Section 1 was at the base of the cochlea while section 1028 was at the apex. Assuming a diameter of 9 μm for each OHC and three parallel rows of OHCs along the guinea pig cochlea (Thorne and Gavin, 1984), each section contained six OHCs. The anatomical width of the guinea pig BM was assumed to increase linearly from 100 μm in the basal region to 200 μm at the apex (Fernández, 1952). Since the OHCs are only spread across a fraction of the BM, their maximal influence over the BM is over an area delimited by the feet of the Deiters' cells (Nilsen and Russell, 2000). As a result of the presence of OHCs and the increasing BM stiffness along the BM width away from the modiolus (i.e., towards the spiral ligament) (Naidu and Mountain, 1998), it is in the organ-of-Corti region that the BM experiences the greatest level of gain. We therefore assumed an effective basilar membrane width that is 0.3 times the anatomical BM width, which also takes into the account the much shorter spatial extent of the RL. Each section was thus 18 μm long and varied from 30 μm to 60 μm in width from base to apex.

To convert the mechanical values described below (stiffness, damping, and mass for the BM and RL) into acoustic analogs, we scaled the parameters to the area of each section to yield the total mechanical impedance and then divided by the square of the area of the section to convert from mechanical impedance to acoustic impedance (Kinsler and Frey, 1962). The OHC stiffness was changed to acoustic terms by multiplying the single OHC stiffness by six to account for the six OHCs per section and dividing by the square of the area of a section. The single OHC overall voltage-to-force gain ($k_f \times k_v$) was also modified in a similar fashion; either one of k_f or k_v could have been converted since it is their multiplicative product that yields a mechanical impedance. The OHC time constant varied with the conductances and capacitances, as described below.

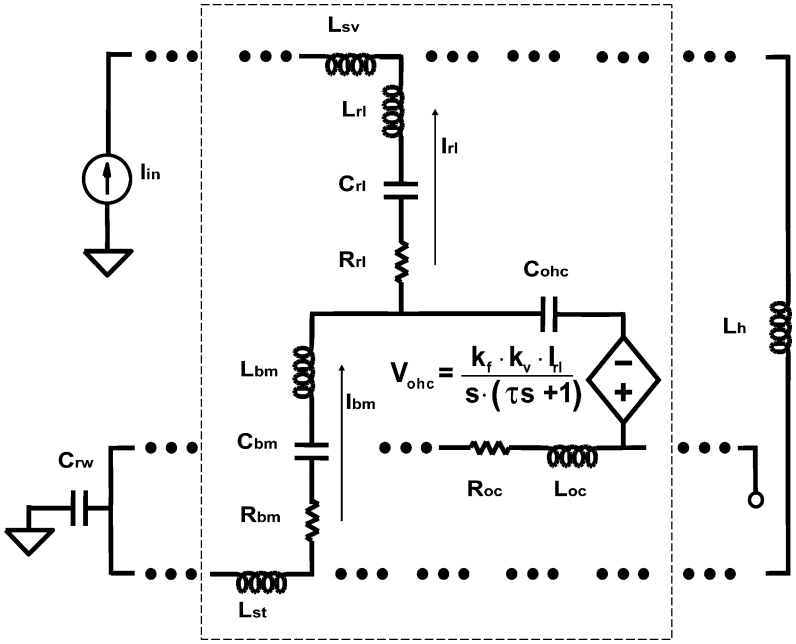

Fig. 7. Macromechanical model of the cochlea composed of local micromechanical sections coupled by fluid. Standard electrical representation of acoustic analogs was used for simulations.

For simulation purposes, we adopted conventional electrical analogs for acoustic elements in Fig. 7 such that current (I) represented volume velocity, voltages (V) were analogous to pressure, inductors (L) referred to acoustic mass (M), resistors (R) represented acoustic damping (R), and capacitors (C) corresponded to acoustic compliance ($C = k^{-1}$). The OHC force generator was modeled as a current-dependent voltage source as described in Eq. (2). The input into the transmission-line model used to simulate the traveling wave for frequency analysis was a velocity source at the oval window, represented as a current source in Fig. 7. The helicotrema was modeled as a mass, the round window was represented as a compliant structure, and the organ of Corti was terminated at the basal end into the round window and at the apical end into an open circuit. A pressure impulse, modeled as a voltage source at the oval window, was used in transient simulations that were performed to ensure model stability. Macromechanical simulations were carried out using Tanner T-Spice® Version 9. All data were processed in Matlab® 6.5 and phase responses were unwrapped using the *unwrap( )* function.

2.3. Parameters

We chose biologically realistic parameters from the literature to simulate our model (Table 1). Most parameters were derived from measurements on guinea pigs. Data from other species were used where guinea pig measurements were incomplete and the model output was compared to chinchilla data (Ruggero et al., 1990). Greenwood's function for the guinea pig cochlea was chosen as the characteristic frequency map (Greenwood, 1990). The functions used for OHC length and stereocilia were consistent with experimental measurements on guinea pigs (Housley and Ashmore, 1992; Wright, 1984). This work is an extension of a Master's thesis by T.K.L. completed in one of the authors' laboratories (R.S.) (Lu, 2003) though all derivations relevant to our theory are contained within this paper.

2.3.1. The basilar membrane, reticular lamina, and tectorial membrane

As described above, we adopted a two-resonator model for the BM and the TM-RL complex (Allen, 1980; Mammano and Ashmore, 1993; Zwislocki, 1979). All mechanical parameters for the BM and RL described below were scaled to an area of 625 μm^2 (from 25 μm probe data). We assumed that the compliance of the basilar membrane ($C_{bm} = k_{bm}^{-1}$) increased by 55.6 dB from base to apex, as measured in gerbils, and was 0.182 m/N measured with a 25 μm probe at the base of the cochlea (Emadi et al., 2004). The reticular lamina compliance was calculated assuming that the RL is six times less stiff than the basilar membrane, based on experiments in guinea pigs (Mammano and Ashmore, 1993). The effective BM mass was determined by the characteristic frequency according to the Greenwood function and the BM compliance at every location. Since the mass of the BM itself may be negligible, the effective mass not only includes the BM tissue mass but also the contents of the organ of Corti and fluid inertia that vibrates with the BM. The effective BM mass is a necessary but artificial construct in our and other 1D models to obtain a realistic frequency-place scaling. This construct would not be necessary in a more complex 3D model taking into account surrounding mechanical structures and fluid effects (Kolston, 1999; Steele, 1999).

The effective RL mass was chosen to be five times less than the BM because the RL is directly coupled to the OHC apical face while there is significant fluid and tissue within the organ of Corti between the BM and the basal end of OHCs. Since the RL itself probably does not have significant physical mass, the effective RL mass may also include fluid mass that vibrates with the RL and actual TM mass (Scherer and Gummer, 2004a). The quality factors (Q) used were −3 dB quality factors. The BM and RL damping factors are calculated from the assumed Q values for both resonant subsystems, which were chosen to match experimental passive and active responses. Since damping due to the thin TM-RL gap is likely to be a larger source of drag than BM damping, the BM quality factor was set to 6 while the RL quality factor was set to 4 at the basal end of the cochlea (Ospeck et al., 2003). The parameter Q_{rl} at the base of the cochlea compares favorably with an estimate of damping based on realistic parameters assuming that the TM-RL gap can be modeled by two parallel plates with viscous fluid in between (Ospeck et al., 2003); i.e., where

$$R_{rl} \approx \frac{\eta \times A}{H_{cilia}} \tag{7}$$

where $\eta = 1.97$ mPa · s is the viscosity of the endolymphatic fluid that fills the gap (von Békésy, 1960), A is the surface area for one of the plates, and H_{cilia} is the gap height with the tallest OHC stereocilia embedded in the tectorial membrane. Eq. (7) yields an estimated R_{rl} of 8.83×10^{-7} N · s/m in model Section 1 while our assumed value Q_{rl} of 4 gives an R_{rl} of 9.12×10^{-7} N · s/m. We used lower limits for the quality factor for simplicity and to demonstrate that our model can perform amplification in highly damped conditions. A lower Q means that larger OHC gains are required to drive the system unstable. Reducing the high levels of assumed damping (i.e. higher Q) would allow us to reduce the OHC gain further. Since the quality factors in the apical end are lower than in the basal end, we exponentially scaled both Q_{rl} and Q_{bm} to decrease by a factor of ten towards the apex (Robles and Ruggero, 2001). Since no comprehensive experimental data was available to determine how we should taper Q_{rl} and Q_{bm}, we chose to decrease both by a factor of ten based on reasonable passive responses obtained from our model when the OHC gain was set to zero.

2.3.2. The outer hair cell

The OHC basolateral conductances and membrane capacitances were assumed to depend on the OHC body

length and are consistent with observed values in guinea pigs (Housley and Ashmore, 1992; Preyer et al., 1994, 1996). Though the exact equations we used for OHC conductance and capacitance (as shown in Table 1) were not exactly equal to those determined by Housley and Ashmore (1992), they were very similar. For example, OHC conductance ranged from 42.7 nS to 3.7 nS for the shortest (20 μm) and longest OHCs (80 μm) in our model whereas Housley and Ashmore (1992) state a range of 38.4 nS to 3.3 nS. Similarly, OHC capacitance ranged from 13 pF to 34.4 pF in our model whereas Housley and Ashmore (1992) quote a range of 17.19 pF to 45.57 pF for the shortest and longest cells, respectively. The membrane time constant, τ, was simply derived by dividing the capacitance by the conductance and had a minimum value of 0.3 ms in the basal region. In practice, guinea pig OHCs with membrane time constants of 0.15 ms have been observed (Housley and Ashmore, 1992). Thus, the values we used for the membrane time constant were conservative to emphasize our point that significant speedup is possible even with very slow OHCs.

The OHC compliance gradient was set to scale directly proportionally with OHC length. We assumed that a 60 μm long OHC had a stiffness of 6 mN/m, which is consistent with typical stiffnesses (0.4–8.5 mN/m) measured in vitro for guinea pig OHCs (He and Dallos, 1999). Since the somatic stiffness of OHCs is dependent on the membrane potential, increasing for hyperpolarization and decreasing for depolarization, it is plausible that the cell resting potential sets the OHC stiffness ideally in vivo.

The single OHC RL-displacement-to-voltage gain at DC, k_v, refers to the low-frequency gain from RL displacement to the membrane voltage. The parameter k_v is independent of frequency since we model the membrane time constant explicitly in τ. The parameter k_v was calculated by assuming that the ratio between the RL motion and stereocilia displacement was 1:1, the maximum slope for the open probability of the mouse hair cell transducer channels for a given stereocilia displacement was $0.04\ \mathrm{nm}^{-1}$ (Ospeck et al., 2003), and the open transducer conductance in the basal regions of the cochlea was 28 nS (He et al., 2004). Because the tips of OHC stereocilia are embedded in the TM, we assumed that stereocilia displacement is driven by RL displacement and not RL velocity (Freeman and Weiss, 1990a,b). The positive endolymph potential and the negative OHC resting potential across the stereocilia generate a driving voltage for positive current into OHCs through the stereocilia transducers. This driving current was estimated to be 150 mV from Ospeck et al. (2003). Thus, a 1 nm displacement of the RL results in a 1.12 nS transducer conductance and an input current of 168 pA. Finally, a basolateral conductance of 42 nS was assumed, consistent with guinea pig measurements (Housley and Ashmore, 1992). Since the membrane capacitance at DC is negligible compared to the basolateral conductance, the DC RL-displacement-to-voltage factor is simply given by dividing the input current by the basolateral conductance, yielding $k_v = 4$ mV/nm. We used values derived from basal parameters to calculate k_v since the basal region is where the cochlear amplifier is most significant. The in vivo parameter k_v can be modulated by adaptation in the stereocilia.

The OHC voltage-to-force gain, k_f, is the crucial component that translates membrane receptor potential into a contractile or expansive force. Upper level estimates for k_f range from 0.5 nN/mV to 1.25 nN/mV in guinea pigs (Mountain and Hubbard, 1994; Iwasa and Chadwick, 1992) while experimental data for in vitro guinea pig OHCs has shown k_f to vary anywhere from 0.1 nN/mV to 53 pN/mV from Frank et al. (1999) and Dong et al. (2002). Scherer and Gummer (2004b) recently estimated k_f to be on the order of 50–300 pN/mV and stated that this could be an underestimate based on limitations in their methods. We assumed an upper limit for k_f of 0.5 nN/mV in the most basal section, which agrees with the above estimates, in order to test how slow our OHC membrane time constants could be while still achieving amplification. This maximum value for the OHC gain, k_f, is only for the most basal section and decreases in successive sections away from the base; in addition, the OHC gain we used is an upper limit since our model can still provide amplification with lower gains. As described above, since the values we assumed for τ could be reduced while remaining consistent with experiments, k_f could concomitantly be decreased by a factor of two or more without altering our conclusions (see Section 3). This would place our estimate for k_f within the range estimated by Scherer and Gummer (2004b). In addition, we were able to reduce k_f even further by modifying some of the other parameters, though we made sure to keep these parameters within experimental limits (see Section 3). The parameter k_f can be modulated by changing the resting potential, allowing an additional degree of control in vivo to increase or decrease the effect of cochlear amplification. We also assumed that the voltage-to-force gain of the motor is frequency independent, at least in the auditory frequency range (Frank et al., 1999).

The parameter k_f was set to vary along the cochlea almost exponentially in a similar fashion to the Greenwood function and was decreased towards the apex. The parameter k_f at the apex was 155 times less than k_f at the base. The scaling of k_f is a simplifying assumption in our theory used to generate a stable model at all frequencies; if k_f was tapered much less, the model would be unstable. In the interest of simplicity, we have also not incorporated further differences between the base and apex of the cochlea that would reduce the scaling requirement. Experimental data for the most appropriate and realistic scaling of k_f and k_v are lacking. We could use a combination of scaling in k_f and k_v to make each parameter change less over the length of the cochlea. Since both k_f and k_v depend on various parameters like OHC potential, resting cilia angle, molecular modulators of stereocilia conductance and the OHC motor that are not known definitively in vivo, we simply scaled k_f only and kept k_v constant. For example, if we

assumed even higher damping in the organ of Corti or on the BM or RL in the apical region, the tapering of k_f would be reduced even further.

The resulting OHC gain-bandwidth product (calculated as k_f/τ) is shown in Fig. 8.

2.3.3. The fluid coupling

We modeled the scala tympani, scala vestibuli and media, and organ-of-Corti fluid since these fluids all couple to mechanical movement in the organ of Corti. Fluid coupling in the macromechanical model was modeled using electrical analogs for fluid components in a tapered transmission line, for example as in Hubbard (1993), Puria and Allen (1991), and Shera and Zweig (1991), where the inductance or fluid mass is determined by the length of each section divided by the longitudinal cross-sectional area (Kinsler and Frey, 1962). The helicotrema connects the scala vestibuli and scala tympani at the apical end while the stapes drives the oval window at the scala vestibuli at the basal end. The round window is at the basal end of the scala tympani. Movement of the organ of Corti is coupled into fluid motion in the scala vestibuli and scala media as well as the scala tympani. Organ-of-Corti fluid flow has also been observed (Mountain and Karavitaki, 2003).

Individual local sections were coupled at the TM-RL complex by the scala vestibuli and the scala media and at the BM by the scala tympani. OHC shortening and lengthening compresses and expands the organ of Corti, generating longitudinal fluid movement within the organ of Corti (de Boer, 1990a). Organ-of-Corti fluid coupling was modeled by a viscous element in addition to fluid mass since the small cross-sectional area and the complex ultrastructure of the organ of Corti is expected to yield a greater resistance to flow (de Boer, 1990b).

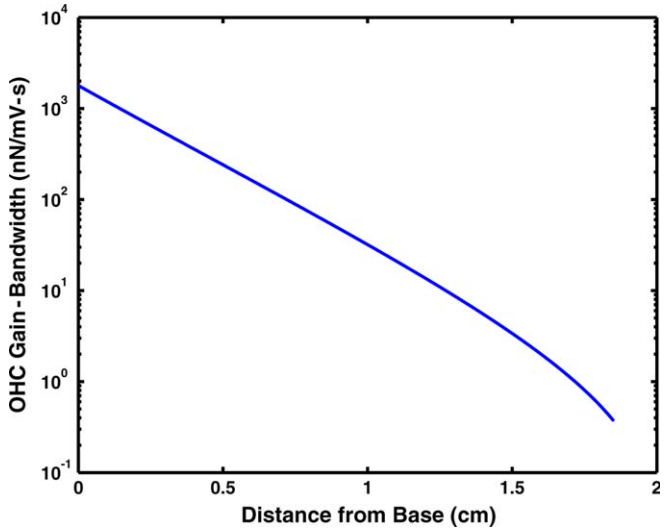

Fig. 8. The OHC gain-bandwidth product used in our simulations shown as a function of distance along the cochlea. The gain-bandwidth product is tapered towards the apex to maintain stability.

The acoustic masses for the fluid compartments coupling the individual sections together were determined using the respective cross-sectional areas. Data from 3D magnetic resonance microscopy reconstruction of the guinea pig cochlea, scaled to the length of the cochlea in our model, were used to determine the cross-sectional areas (Thorne et al., 1999). We created a piecewise function to model the experimental data (Fig. 9). The scala tympani mass is represented in Fig. 7 as L_{st}. The scala vestibuli fluid mass, L_{sv}, included the scala media as well (Fig. 7). We assumed that the effective cross-sectional areas used to calculate L_{st} and L_{sv} were 0.3 times the anatomical cross-sectional areas in Fig. 9 since motion of the fluid near the boundaries of the scalae is reduced. The fluid mass of the organ of Corti, L_{oc}, was determined by assuming that its cross-sectional area was $0.012\,mm^2$ at the base and

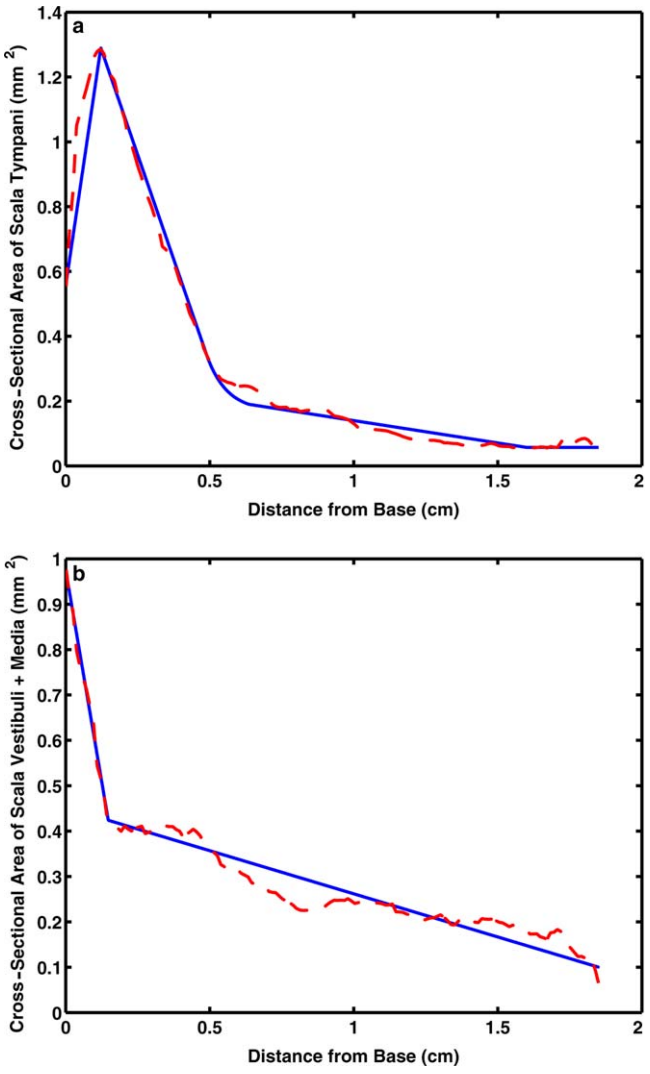

Fig. 9. Experimental (Thorne et al., 1999) (*dashed lines, red*) and piecewise-approximated (*solid lines, blue*) cross-sectional areas of the scalae. Changes in the slope of the scala tapering were found to influence model results. (a) Scala tympani area determined L_{st}. (b) Scala vestibuli and scala media areas were added together to determine L_{sv}. (For interpretation of the references in colour in this figure legend, the reader is referred to the web version of this article.)

increased linearly to 0.017 mm^2 at the apex (Fernández, 1952). The area of the organ of Corti was divided by the anatomical width of the basilar membrane to obtain an effective channel height. The resistance of the organ of Corti, R_{oc}, was calculated assuming fluid flow within a rectangular channel (Deen, 1998). Using the anatomical BM width instead of the effective BM width to calculate R_{oc} yields a shorter height and results in an upper bound on the resistance since R_{oc} is inversely proportional to the height cubed while only inversely proportional to the width.

The scala vestibuli and scala tympani masses were terminated at the apical end by the helicotrema, which was assumed to have a fluid mass, L_h, of 2×10^5 kg/m^4. This value is in between the scala vestibuli fluid mass (1.84×10^5 kg/m^4) and the scala tympani fluid mass (3.22×10^5 kg/m^4) at the apical end. The round window compliance, C_{rw}, given by 1×10^{-13} m^5/N, terminates the basal end of the scala tympani line, consistent with measurements in cats (Lynch et al., 1982). The organ-of-Corti line was left open-circuited at the apical end while it was terminated into the round window at the basal end to ensure that there was equal volume displacement at the round and oval windows, thus maintaining overall cochlear incompressibility (Stenfelt et al., 2004). The appropriate termination of the organ-of-Corti line is not well characterized experimentally, but terminating the apical end into the helicotrema did not cause notable changes as far as basal responses were concerned (Puria and Allen, 1991). The conversion factor from volume velocities to linear velocities needed to calculate the basilar-membrane-to-stapes motion ratio was determined by dividing the oval window area (0.961 mm^2, given by the initial area of the scala vestibuli as measured by Thorne et al. (1999)) by the area of the relevant section.

3. Results

Micromechanical simulations were performed using the model parameters from Table 1 for the most basal section of the cochlea, where the characteristic frequency is 43.6 kHz in the guinea pig (Wilson and Johnstone, 1975) and active cochlear amplification is needed for high-frequency hearing. Negative feedback increases the open-loop pole corresponding to the membrane time constant from 522 Hz to 7.46 kHz for realistic OHC gains at the most basal section and thus reduces the membrane time constant cutoff ($k_f = 0.5$ nN/mV). This pole is still a factor of 5.8 off from the required CF of 43.6 kHz (Fig. 10a). However, negative feedback also increases the BM and RL resonant gain, thus permitting adequate OHC force near resonance (Fig. 10a). Due to the −3 dB OHC cutoff from the time constant, resonance alone, without adequate OHC feedback gain, is not enough to yield a sufficient force (Fig. 10a).

Root locus plots illustrate how closed-loop poles (or singularities) of the system move with increasing loop gain. The root locus plot in Fig. 10b shows that, consistent with the magnitude plot shown in Fig. 10a, the OHC membrane time constant, represented as a pole on the real axis, moves away from the origin with increasing OHC gain and has a decreasing effect on the system. Furthermore, increasing OHC gain moves a pair of complex poles towards the imaginary axis, which results in increased resonant gain. Fig. 11 shows the root locus plot

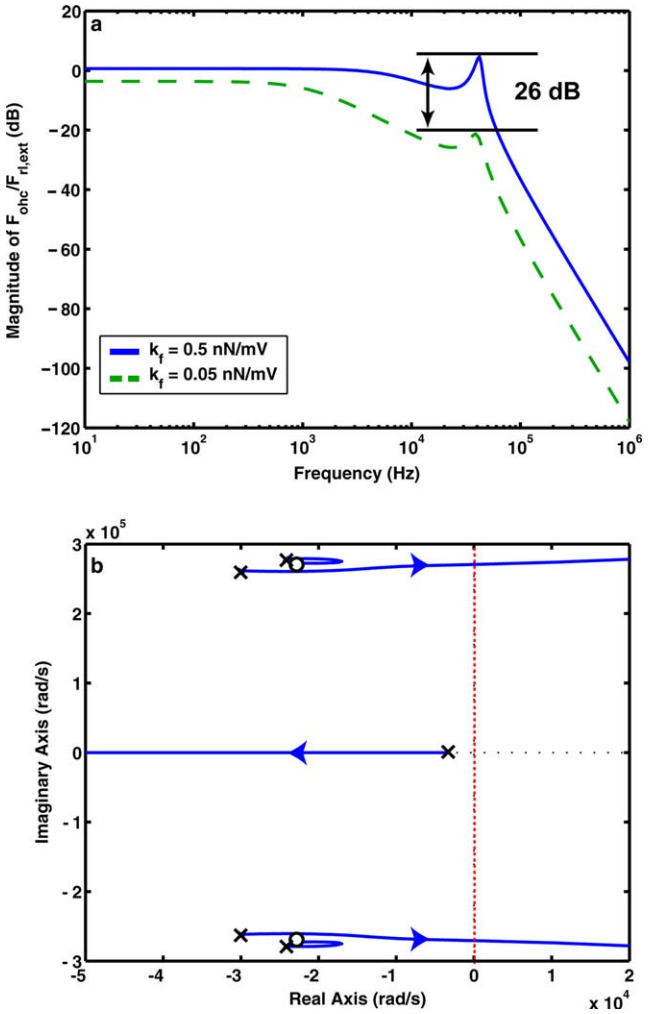

Fig. 10. Results from simulation of the micromechanical model of the cochlea (a) Magnitude plot of the transfer function from $F_{rl,ext}$ to the OHC force generator, F_{ohc}. Higher k_f values reduce mid-frequency roll-off and increase resonant gain, making the OHC force effective in amplifying the mechanical response at resonance. Decreasing the OHC gain by a factor of 10 generates a 26 dB drop in the resonant OHC force, lowers the low-frequency asymptote, and changes the "tip-to-tail" ratio from +4.7 to −21.3 dB. (b) Root locus plot (where x = poles of the system, o = zeros of the system, and axes are in units of rad/s) of the loop gain (absolute value of Eq. (6)) demonstrates that as the OHC gain is increased, the pole on the real axis that represents the OHC membrane time constant moves further away from the origin and thus has less effect on the system. Furthermore, whereas one pair of complex poles travels towards the pair of complex zeroes, the other pair of complex poles moves towards the imaginary $j\omega$ axis (*dashed line*, *red*) as the OHC gain increases, thus increasing resonant gain of the system. (For interpretation of the references in colour in this figure legend, the reader is referred to the web version of this article.)

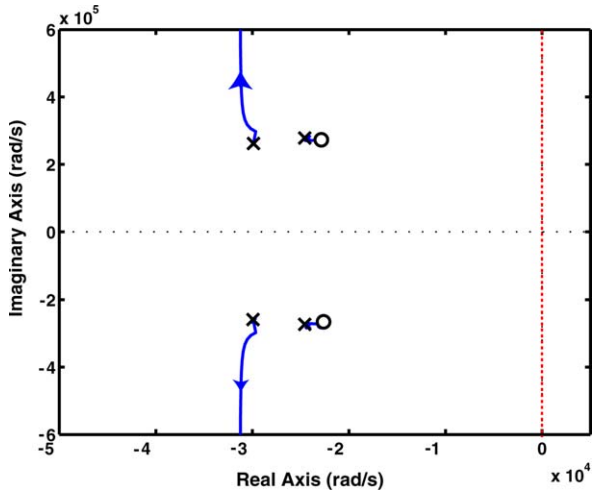

Fig. 11. Root locus plot of the loop gain (absolute value of Eq. (6)) where the membrane time constant is set to zero shows that as the OHC gain is increased, one pair of complex poles travels toward the pair of complex zeroes while the other pair of complex poles moves almost parallel to the imaginary axis. This motion is in contrast to the root-locus plot shown in Fig. 10 where the motion of one pair of poles is almost perpendicular to the imaginary axis such that the membrane time constant actually assists in increasing the mechanical resonant gain more effectively.

with no outer hair cell membrane time constant. In contrast with Fig. 10b, the complex poles in Fig. 11 do not move towards the imaginary axis and instead move almost parallel to it, implying that the resonant gain of the system, determined by the angle of the pole vector with respect to the imaginary axis, is not increased by as much. Thus, the membrane time constant provides a phase shift that actually assists in increasing the mechanical resonant gain by causing motion of the poles towards the imaginary axis rather than parallel to it.

Therefore, an increase of the OHC cutoff frequency along with increased resonance due to negative feedback are both necessary for adequate OHC force near resonance. Very high OHC gains can drive the system unstable. Thus, one cannot draw conclusions about the closed-loop high-frequency response of the cochlear feedback circuit simply by looking at the open-loop OHC bandwidth; *instead, the OHC gain and OHC bandwidth must both be known along with the passive mechanical components that affect the loop transmission. It is the OHC gain-bandwidth product and these passive mechanics together that determine if high-frequency amplification is possible.*

Simulations of the macromechanical model used parameters that were biologically realistic (Table 1) and were scaled to volume velocity and pressure units. In Section 2.3, we described how we chose these parameters. Transient time simulations were performed to ensure that the model was stable.

The magnitude (Fig. 12a) and phase (Fig. 12b) of the input/output response at section 320 (5.76 mm from the base, with Section 1 at the base) closely match experimental data obtained from chinchilla (Ruggero et al., 1990). The magnitude (Fig. 12a) peaks at 9.13 kHz. By increasing

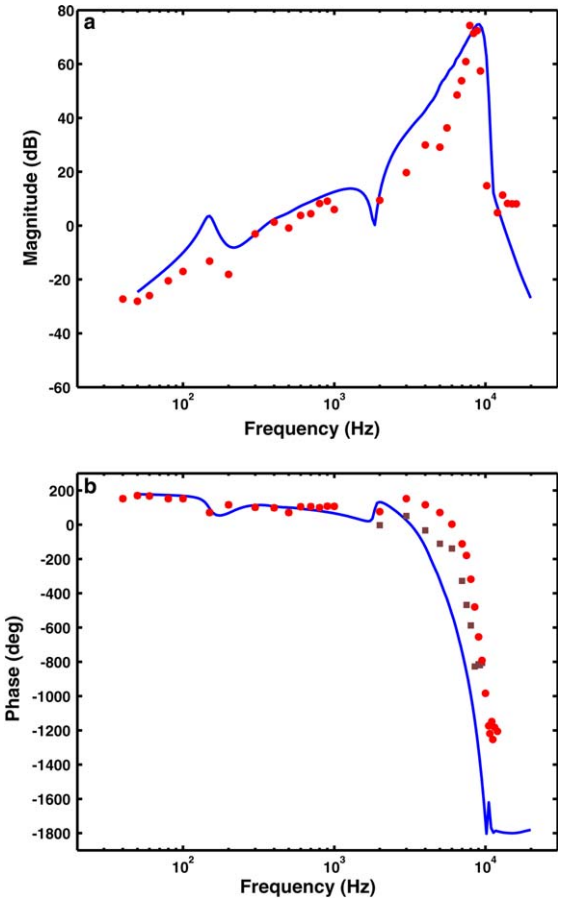

Fig. 12. Results from simulation of the macromechanical model of the cochlea composed of local micromechanical sections coupled by fluid. (a) BM-to-stapes-velocity ratio from the model at section 320 (*solid line, blue*) compares favorably with experimental chinchilla data (Ruggero et al., 1990) (*red circles*). Volume velocity to linear velocity conversion is 62.7 dB. (b) Phase response from the model matches experimental results (Ruggero et al., 1990) (*red circles*, *brown squares*). Note that the experimental phase data shows "the full range of variation in BM phase data" (Ruggero et al., 1990) and is not drawn from the same animal as the magnitude data in (a). (For interpretation of the references in colour in this figure legend, the reader is referred to the web version of this article.)

the OHC gain by a factor of 1.35 over the values used in Table 1, greater than 70 dB of active gain over the passive peak can be achieved (not shown). Note that the experimental phase data shows "the full range of variation in BM phase data" (Ruggero et al., 1990) and is not drawn from the same animal as the magnitude data in Fig. 12a.

Fig. 13 shows the magnitude and phase of the passive macromechanical model. The dotted black curves in Fig. 13 represent the case where the OHC gain was reduced to $k_f = 0$. We note a phase plateau of $-353°$ and the peak magnitude response with active amplification is greater than 45 dB compared with the passive case. The solid blue curves in Fig. 13 show a phase plateau with $-624°$ and a 54 dB difference in active versus passive amplification. Like the points of the dotted-black curves, the points of the solid blue curves were also obtained by lowering the OHC gain, k_f, to 0 nN/mV but in addition, the effective BM width

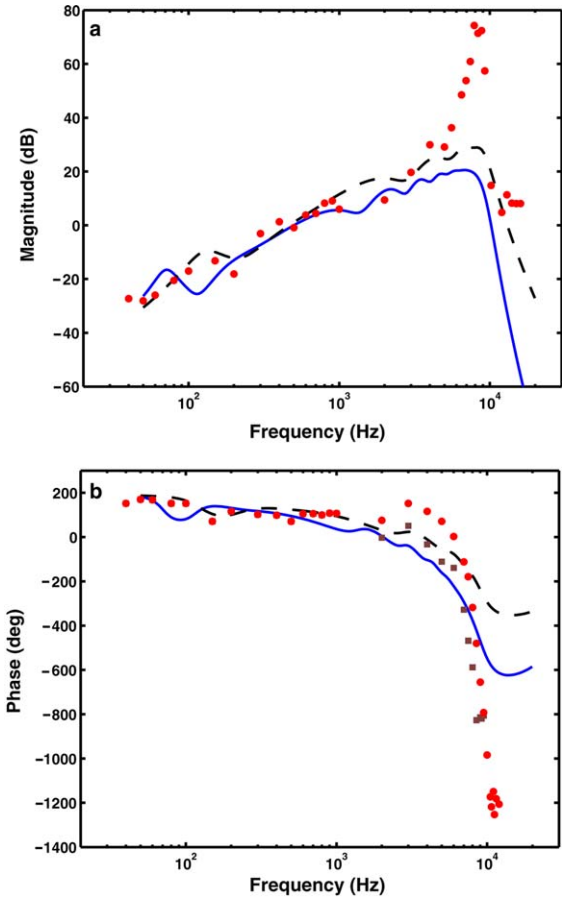

Fig. 13. Results from simulation of the passive macromechanical model ($k_f = 0$ nN/mV). (a) BM-to-stapes-velocity ratio from the model at section 320 with an effective BM width equal to 0.3 times the anatomical BM width (*dashed line, black*) and BM-to-stapes-velocity ratio at section 320 with an effective BM width equal to the anatomical BM width (*solid line, blue*). Volume velocity to linear velocity conversion is 62.7 dB in the former passive case; the magnitude difference between the active cochlea in Fig. 12a and the former passive case is over 45 dB. Volume velocity to linear velocity conversion is 52.3 dB in the latter passive case; the magnitude difference between the active cochlea in Fig. 12a and the latter passive case is over 54 dB. Active experimental chinchilla data (Ruggero et al., 1990) is also plotted (*red circles*). (b) Phase response from the model at section 320 with an effective BM width equal to 0.3 times the anatomical width (*dashed line, black*) and phase response at section 320 with an effective BM width equal to the anatomical BM width (*solid line, blue*). The former passive case reaches a phase of about −353° at high frequencies while the latter passive case reaches a phase of about −624° at high frequencies. Active experimental chinchilla data (Ruggero et al., 1990) is also plotted (*red circles*, *brown squares*). Note that the experimental phase data shows "the full range of variation in BM phase data" (Ruggero et al., 1990) and is not drawn from the same animal as the magnitude data in (a). (For interpretation of the references in colour in this figure legend, the reader is referred to the web version of this article.)

described in Section 2.2 was increased to be equal to the anatomical BM width. According to Kolston (1999), when OHC motility is absent, motion across the entire width of the BM is significant; therefore, in the passive cochlea, the extent of the entire BM should be reflected in the 1D model rather than just the region near the Deiters' cells as in the active case (Nilsen and Russell, 2000). Not surprisingly, the solid blue curves fit experimental data for the passive case better and have phase plateaus near the post-mortem adult phase plateaus reported in Overstreet et al. (2002) and Ren and Nuttall (2001). The peak shifts with respect to the active case in both the dotted black and the solid blue curves of Fig. 13 are 0.39 octaves and 0.41 octaves, respectively. These shifts are not unlike experimentally observed intensity-dependent peak shifts. Our findings illustrate that 2D or 3D modeling of the cochlea as well as more detailed micromechanical models are essential in obtaining accurate fits to data (Kolston, 1999; Steele, 1999). They also illustrate that a set of parameters rather than a single parameter is likely to change when moving between the active and passive cases.

Fig. 14 shows outputs from sections 100, 200, 300, 400, 500, 600, 700, 800, 900, and 1000, which are spaced apart by 1.8 mm each. Outputs towards the base (i.e. sections 100 and 200) have decreased peak magnitude responses, a trend also seen in experimental data (Robles and Ruggero, 2001). Our model is able to achieve about at least 46 dB of gain at section 100 (CF ~ 24.5 kHz) and 61 dB of gain at section 200 (CF ~ 15.8 kHz), which corresponds well to ~48 dB (CF ~ 30 kHz in cat) and ~58 dB (CF ~ 17 kHz in guinea pig) measured by Cooper and Rhode (1992) and Sellick et al. (1983), respectively. Furthermore, the phase rolls off less as one looks at sections closer to the basal end, a trend also seen in experimental data (Robles and Ruggero, 2001). The model behaves very differently at the apex (i.e. sections 800, 900, 1000) compared to the basal sections, showing a much broader magnitude peak and less phase roll off (Fig. 14). Magnitude gains of about ~28 dB and ~15 dB were obtained in sections 900 and 1000, respectively, which correspond well with experimental evidence (Robles and Ruggero, 2001). These results demonstrate that our model fits a range of experimental data relatively well, even though we only concentrated our modeling efforts on the basal region.

As mentioned in Section 2.3.2, we were able to reduce k_f from its maximum value of 0.5 nN/mV in the most basal section by either reducing the OHC time constant or modifying other model parameters. Since we assumed a maximum OHC RC cutoff frequency of 522 Hz in the basal end but experimental data has shown that the RC cutoff frequency constant can reach 1 kHz in the basal end (Housley and Ashmore, 1992; Preyer et al., 1996), we ran our model with new OHC time constants that were equal to half of what they were before (i.e., twice the OHC RC cutoff frequency) and new k_f values that were half of what they were before (i.e. $k_f = 0.25$ nN/mV at most basal section). The output from section 320 with these new parameters (Fig. 15) closely matches the output from the model with the original parameters (Fig. 12).

The OHC gain, k_f, can also be reduced by modifying other model parameters such as the BM stiffness. We reduced BM stiffness by a factor of 5.5, well within the measurement limits described by Emadi et al. (2004) and

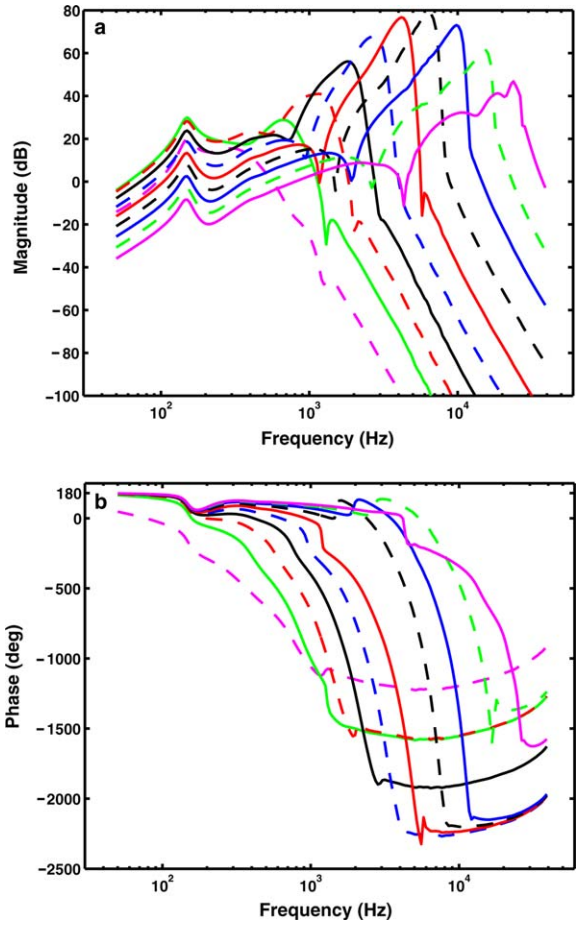

Fig. 14. Results from simulation of the macromechanical model of the cochlea composed of local micromechanical sections coupled by fluid at (in order from right to left) sections 100 (1.8 mm from stapes, *solid line*, *magenta*), 200 (3.6 mm from stapes, *dashed line*, *green*), 300 (5.4 mm from stapes, *solid line*, *blue*), 400 (7.2 mm from stapes, *dashed line*, *black*), 500 (9 mm from stapes, *solid line*, *red*), 600 (10.8 mm from stapes, *dashed line*, *blue*), 700 (12.6 mm from stapes, *solid line*, *black*), 800 (14.4 mm from stapes, *dashed line*, *red*), 900 (16.2 mm from stapes, *solid line*, *green*), and 1000 (18 mm from stapes, *dashed line*, *magenta*). (a) BM-to-stapes-velocity ratios with respective volume velocity to linear velocity conversion. The magnitude response towards the apex (i.e. sections 800, 900, 1000) are drastically different than those towards the base. (b) Phase responses also show vivid differences between the apex and the base.

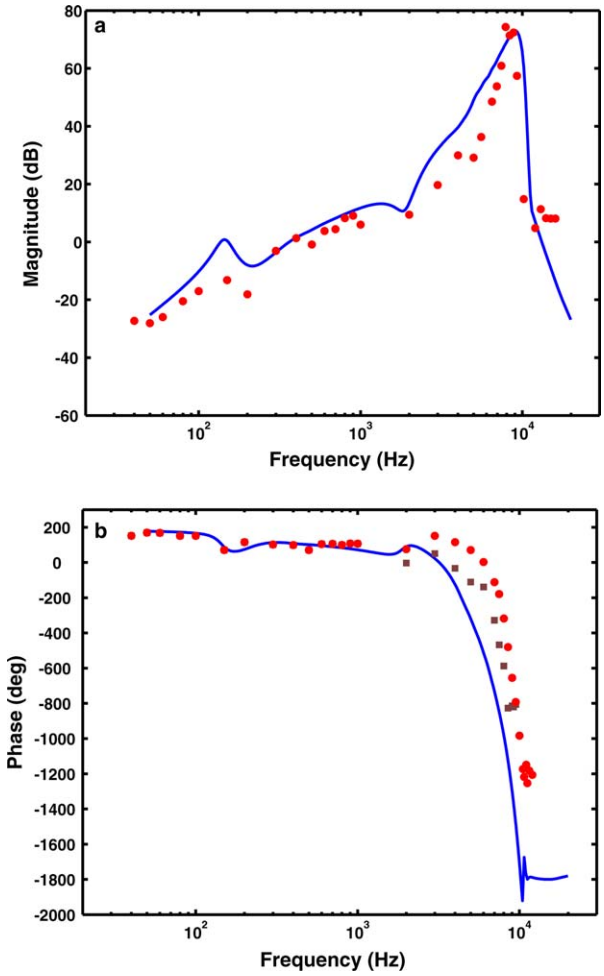

Fig. 15. Results from simulation of the macromechanical model with new OHC time constants equal to half of what they were in Fig. 12 (max OHC cutoff frequency = 1 kHz) and k_f reduced to half of what they were in Fig. 12 (max $k_f = 0.25$ nN/mV) demonstrate that it is the gain-bandwidth product that is key to amplification with the OHC time constant and not the gain or the bandwidth alone. These results also demonstrate that the OHC gain, k_f, can be reduced considerably in our model. (a) BM-to-stapes-velocity ratio from the model at section 320 (*solid line, blue*) compares favorably with experimental chinchilla data (Ruggero et al., 1990) and is almost identical to Fig. 12a (*red circles*). Volume velocity to linear velocity conversion is 62.7 dB. The magnitude difference between the passive case ($k_f = 0$ nN/mV and no change in effective BM width) and the active case is over 43 dB. (b) Phase response from the model matches experimental results (Ruggero et al., 1990) and is almost identical to Fig. 12b (*red circles*, *brown squares*). (For interpretation of the references in colour in this figure legend, the reader is referred to the web version of this article.)

concomitantly reduced the OHC gain by a factor of 4.17 (reduced maximum k_f from 0.5 nN/mV to 0.12 nN/mV). The output from section 320 with these new parameters (Fig. 16) shows that although the fit to data is not as good as in Fig. 12, a broad magnitude response can still be obtained with over 44 dB of gain compared to the passive case, where $k_f = 0$ nN/mV and there was no change in effective BM width (data not shown). This demonstrates that much smaller OHC gains can still produce amplification in the cochlea in our model. Thus, there is sufficient gain-bandwidth in the OHC to overcome the membrane RC time constant.

Our model is consistent with experimental observations in which OHC damage, which presumably lowers OHC gain, resulted in less sensitive auditory-nerve tuning-curve tips and hypersensitivity of tuning-curve tails (Liberman and Dodds, 1984). OHCs provide mechanical amplification, lowering auditory-nerve thresholds near the tip region; thus, OHC damage shortens tuning-curve tips. Negative feedback at low frequencies clamps or "servos" RL movement to a minimum since any motion generates an opposing motion; higher OHC gains clamp the RL more efficiently. OHC damage allows the RL to move more near the low-frequency tail region (not shown), leading to the hypersensitivity of tuning-curve tails, assuming that

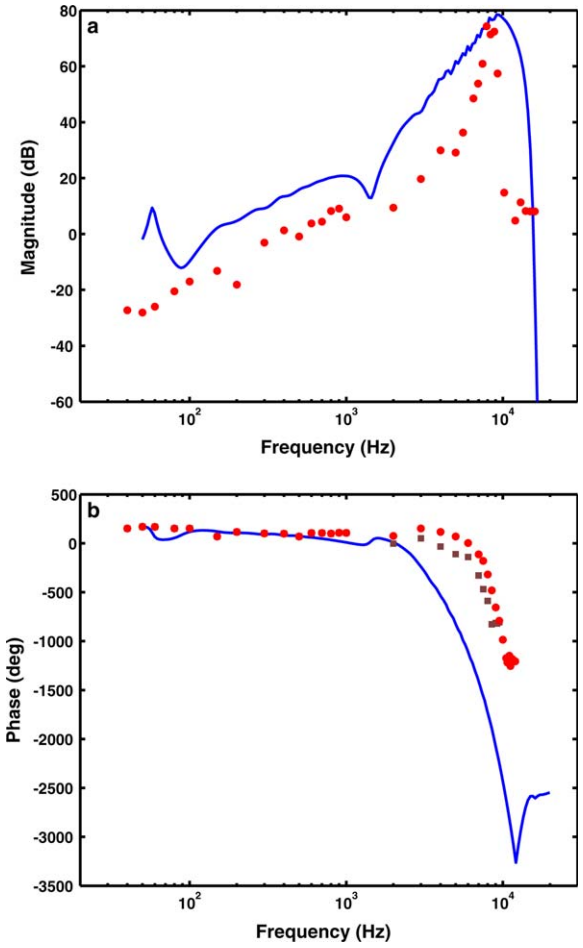

Fig. 16. Results from simulation of the macromechanical model with BM stiffness reduced by a factor of 5.5 ($k_{bm} = 1$ N/m or $C_{bm} = 1$ m/N at the basal end) and OHC gain reduced by a factor of 4.17 (max $k_f = 0.12$ nN/mV at the basal end) demonstrate that the OHC gain, k_f, can be reduced considerably in our model by reducing the BM stiffness within experimental limits (Emadi et al., 2004). (a) BM-to-stapes-velocity ratio from the model at section 320 (*solid line, blue*) compares favorably with experimental chinchilla data (Ruggero et al., 1990) and has a broader peak compared with Fig. 12a (*red circles*). Volume velocity to linear velocity conversion is 62.7 dB. The magnitude difference between the passive case ($k_f = 0$ nN/mV and no change in effective BM width) and the active case is over 44 dB. (b) Phase response from the model rolls off faster compared to experimental results (Ruggero et al., 1990) and Fig. 12b (*red circles*, *brown squares*). (For interpretation of the references in colour in this figure legend, the reader is referred to the web version of this article.)

RL motion controls auditory-nerve stimulation via inner hair cells. Lowering OHC gain by other mechanisms, such as salicylate (Fitzgerald et al., 1993) or efferent fiber stimulation (Guinan and Gifford, 1988; Murugasu and Russell, 1996), should lead to similar observations. In addition, to maintain stability in our model, the OHC gain-bandwidth product should decrease from base to apex of the cochlea. The open-loop OHC bandwidth has been observed to decrease towards the apex (Housley and Ashmore, 1992; Preyer et al., 1996). Impedance discontinuities in the model produce instability, which is consistent with micro-lesions in the cochlea generating spontaneous otoacoustic emissions (Shera, 2003; Zweig and Shera, 1995; Talmadge et al., 1998).

Although the TM was not explicitly modeled, the TM is important in forcing the stereocilia displacement to be proportional to the RL displacement due to the embedding of OHC stereocilia tips in the TM. The TM may resonate near the CF and generate larger stereocilia displacements near resonance (Gummer et al., 1996). In our model, the scala vestibuli and scala media pressure are assumed to act directly upon the TM-RL complex through the TM. This is justified by the observation that TM motion is largely perpendicular to RL motion (Ulfendahl et al., 1995) and, due to the thin subtectorial gap, the motions of the TM and RL are expected to be coupled (Chadwick et al., 1996). Furthermore, the TM may be crucial for transmitting vibrations from the OHCs to stimulate inner hair cells. Future work comparing TM, RL, and inner hair cell responses from our model to neural tuning curves may yield further insight into the complex micromechanics of the cochlea.

3.1. Collective amplification in the macromechanical model

The cochlea's traveling-wave nature means that any single section's resonant gain need not be high because numerous individual OHCs over a limited spatial extent collectively contribute to the output. An active region of about 3.06 mm basal to the peak is necessary to obtain a peak gain of 50 dB based on the parameters we used. We determined the necessary active region by removing the active force generator in successively more consecutive sections starting with Section 1 until the peak gain dropped below 50 dB. We chose 50 dB as a threshold because the model transfer function remained fairly sharp and selective and still had sufficient gain over the passive case. Increasing the active gain by a factor of 1.285 reduces the necessary active region for the same peak gain to about 1.44 mm. Thus, by increasing the OHC gain we can reduce the necessary active region of cumulative gain in our model. A higher-order micromechanical resonator model or a model that incorporates higher-order dimensionality of the fluid chambers than we have used can further reduce the necessary region of active gain to more closely match experimental data. For example, if we use an increased active gain (by a factor of 1.285) as described above and a two-dimensional model with ten sections to model the vertical spatial extent of the scala tympani and the scala vestibuli + media fluid lines, the necessary active region for a peak gain of 50 dB can be reduced to 1.26 mm. Most estimates for the region of active gain fall within ~1–2 mm basal to CF (Nilsen and Russell, 2000; Robles and Ruggero, 2001; de Boer and Nuttall, 2000). There have been reports in the literature that the region of active gain may be even less than 0.5 mm in the cochlea (Cody, 1992). Our model, in its current form, does not yield such a small region of active gain. Nevertheless, it still sheds insight on the OHC speedup problem. Future work with more complex models is needed to faithfully reproduce all experimental results.

Although section-to-section gains are low (Fig. 17a), the output gain, which is the product of the gains of all the preceding stages, is large (Fig. 17b). Incremental local changes can cause large changes in the overall network output by collective interaction; for example, a minor gain reduction (~1 dB) between every 10 sections (Fig. 17a vs. c) leads to a much larger reduction (~12 dB) in the overall gain (Fig. 17b). Hence, the theory presented here does not require large speedups or gain increases at any local OHC stage or for any single OHC because the traveling-wave architecture of the cochlea provides amplification over numerous OHCs. The advantages of collective amplification have been described in Sarpeshkar et al. (1998) and Sarpeshkar (2000). Collective amplification has also been described in Geisler and Sang (1995), Steele (1999), and Lim and Steele (2002) in feedforward models of the cochlea, where apically-tilted OHCs sense incoming acoustic waves and create forces to counteract damping to create amplification. In comparison, our model is a feedback model. In engineering, feedforward systems allow designers to avoid stability issues but are less robust to variability in the parameters of the system; in contrast, feedback systems must be properly designed to avoid instability but benefit from the increased robustness to component variations provided by negative feedback. To our knowledge, none of the proposed feedforward models have provided mechanisms or an explanation for how the time-constant limitation of the OHCs is overcome.

3.2. Piezoelectricity

OHC motor piezoelectricity may decrease the membrane time constant, which would reduce the OHC gain required by our model (Spector et al., 2003; Weitzel et al., 2003; Spector, 2005; Spector et al., 2005). In addition, the piezoelectric effect itself constitutes a minor negative-feedback loop that increases the OHC stiffness and force gain and makes the negative-feedback loop more effective. By doing so, piezoelectricity helps further extend the OHC bandwidth.

We focus on the effect of electrical piezoelectric properties on mechanical dynamics as opposed to other work that emphasizes the effect of mechanical piezoelectric properties on electrical dynamics (Mountain and Hubbard, 1994; Spector et al., 2003; Weitzel et al., 2003; Spector, 2005; Spector et al., 2005). This choice is necessary and more natural for modeling mechanical cochlear transfer functions with electrical variables serving as intermediate variables. However, both methods are valid for modeling purposes and are consistent with each other. We do not ignore electrical effects but simply account for them mechanically. The piezoelectric properties of the OHC motor are characterized by two constitutive equations (Fig. 18) (Dong et al., 2002):

$$I_{\text{piezo}} = sC_{\text{m}}v_{\text{m}} + sc_{12}F_{\text{ohc,ext}} \tag{8}$$

$$U_{\text{ohc}} = sc_{21}v_{\text{m}} + \frac{s}{k_{\text{ohc}}}F_{\text{ohc,ext}} \tag{9}$$

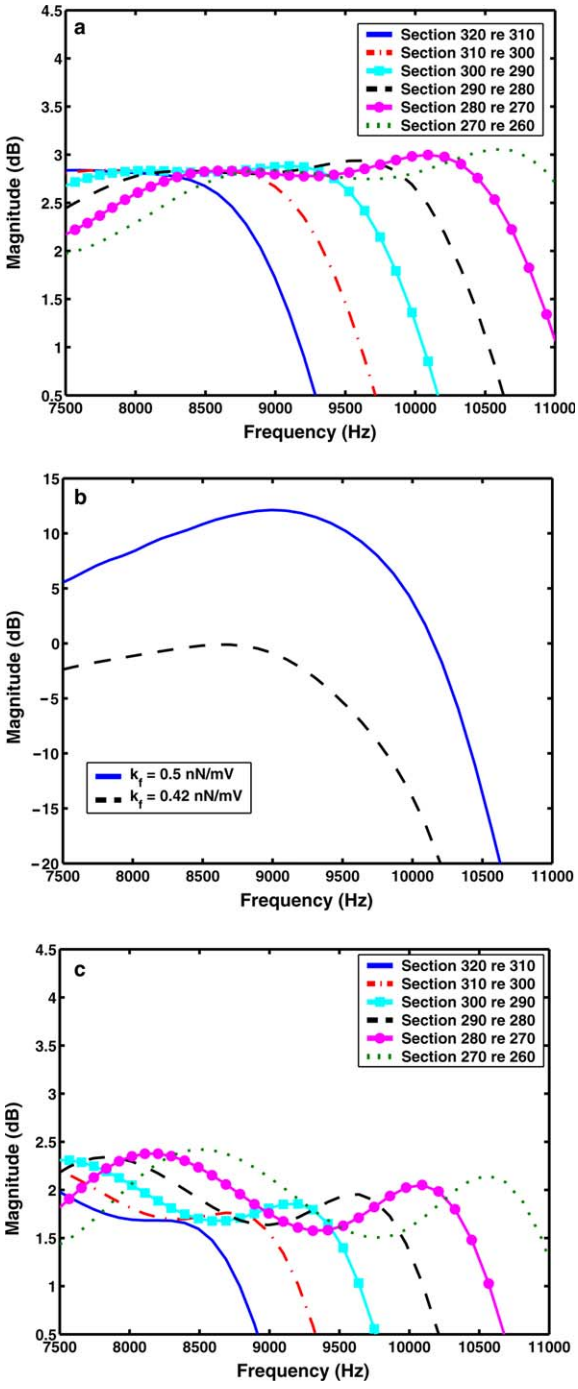

Fig. 17. Simulations demonstrating collective traveling-wave architecture of the cochlear model. (a) and (c) The volume velocity ratios between every ten micromechanical sections from section 270 to section 320 for (a) normal k_f values as described in Table 1 (i.e. Section 1 $k_f = 0.5$ nN/mV) and (c) reduced k_f by a factor of 0.84 from normal (i.e. Section 1 $k_f = 0.42$ nN/mV). The frequency axis is plotted linearly over a narrow range. Small changes in the local OHC k_f (~1 dB from (a) to (c)) can have substantial impact on the overall traveling-wave gain (~12 dB in (b)). (b) The stapes-volume-velocity-to-BM-volume-velocity overall transfer function at section 320 for normal k_f values as described in Table 1 (i.e. Section 1 $k_f = 0.5$ nN/mV) (*solid line, blue*) and reduced k_f by a factor of 0.84 from normal (i.e. Section 1 $k_f = 0.42$ nN/mV) (*dashed line, black*). Note that the normal k_f (i.e. Section 1 $k_f = 0.5$ nN/mV) case in (b) is identical to Fig. 12a but shows a lower absolute gain since the linear-velocity-to-volume-velocity conversion was not performed.

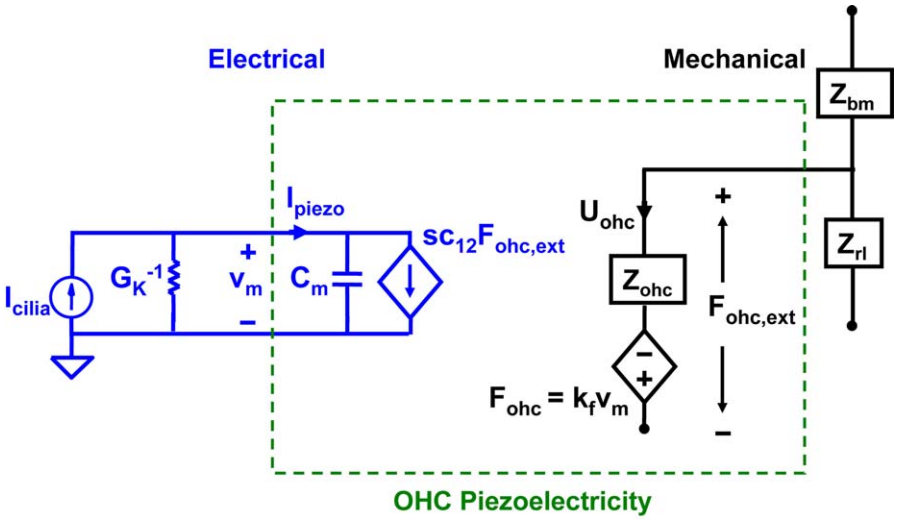

Fig. 18. Piezoelectric effects in the OHC couple its electrical and mechanical variables. In our model described in the main text, we do not account for the mechanical-to-electrical coupling (the $sc_{12}F_{ohc}$ current source in the electrical side) as we now do here. The $k_f v_m$ voltage source in the mechanical side is the electrical-to-mechanical coupling. The membrane voltage is v_m. The velocity of the OHC, U_{ohc}, is defined positive for contraction. The externally applied force, $F_{ohc,ext}$, on the OHC is defined positive if it causes contraction and generates an outwards OHC current that tends to depolarize the cell. The membrane voltage is v_m. The input current due to stereocilia ion currents is I_{cilia}. The OHC mechanical impedance Z_{ohc} is given by Eq. (5). The piezoelectric coefficient is positive because a positive v_m causes contraction, increasing U_{ohc}, and a positive $F_{ohc,ext}$ causes current to be displaced out of the OHC (Dong et al., 2002).

By Maxwell reciprocity for piezoelectricity, $c_{12} = c_{21}$. These two parameters are the piezoelectric coefficient and are positive for our adopted conventions (Fig. 18). The parameter we defined as $k_f = c_{21} \cdot k_{ohc}$ was the OHC voltage-to-force gain when we ignored the c_{12} term in Eq. (8), where c_{21} is the piezoelectric coefficient and k_{ohc} is the passive OHC stiffness. Note that Fig. 18 is exactly the same as the micromechanical model described in the main text except that we have now included the mechanical-to-electrical coupling (the $sc_{12}\,F_{ohc}$ current source).

To determine the effect of the piezoelectric mechanical-to-electrical coupling due to c_{12} on the OHC mechanical properties, we substitute $I_{piezo} = -v_m \cdot G_K + I_{cilia}$ from Fig. 18 into Eqs. (8) and (9) and find:

$$U_{ohc} = \frac{sc_{21}I_{cilia}}{G_K(\tau s+1)} + \left(\frac{s}{k_{ohc}} - \frac{s^2 c_{12}c_{21}}{G_K(\tau s+1)}\right)F_{ohc,ext} \qquad (10)$$

Eq. (10) can be simplified by defining the effective OHC mechanical admittance:

$$Y_{ohc,eff} = \frac{1}{Z_{ohc,eff}} = \left.\frac{U_{ohc}}{F_{ohc,ext}}\right|_{I_{cilia}=0} = \frac{s}{k_{ohc}} - \frac{s^2 c_{12}c_{21}}{G_K(\tau s+1)} \qquad (11)$$

The first term in Eq. (11) is the passive OHC compliance while the second term is an effective admittance due to the mechanical-to-electrical coupling. We rearrange Eq. (10) using Eq. (11) and substitute for the stereocilia ion current $I_{cilia} = k_v\, G_K\,(U_{rl}/s)$ to show that:

$$F_{ohc,ext} = -\frac{c_{21}k_v U_{rl}}{Y_{ohc,eff}(\tau s+1)} + \frac{U_{ohc}}{Y_{ohc,eff}} \qquad (12)$$

Since Eq. (12) decomposes the total OHC force $F_{ohc,ext}$ into a component due to RL motion (first term on right-hand-side) and another component due to the OHC passive mechanical admittance (second term on right-hand-side), we develop a complete model that incorporates the electrical variables into the mechanical variables (Fig. 19). Fig. 19 represents a single section in the traveling-wave model shown in Fig. 7. The mechanical-to-electrical coupling variable c_{12} adds additional mechanical elements in parallel to the passive OHC compliance, as outlined in Fig. 19. At low

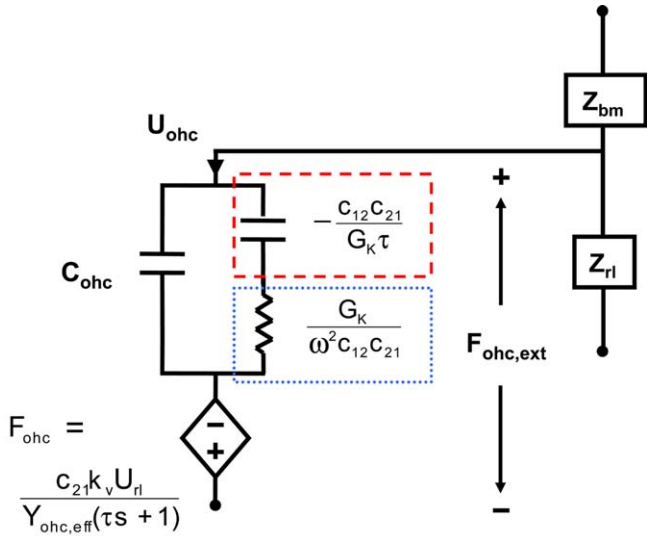

Fig. 19. The effective mechanical circuit after including the mechanical-to-electrical coupling variable c_{12} is modified by the new effective OHC mechanical admittance $Y_{ohc,eff}$. Including c_{12} adds a negative compliance (*dashed line, red*) in series with a viscous element (*dotted line, blue*) both in parallel to the passive OHC compliance, based on Eq. (11). This model reduces to the simpler model used in the main text when $c_{12} = 0$. (For interpretation of the references in colour in this figure legend, the reader is referred to the web version of this article.)

frequencies ($\omega \ll 1/\tau$) in Fig. 19, the viscous or resistive element (dotted line, blue) has a larger impedance and dominates over the negative-compliance element (dashed line, red). At high frequencies, ($\omega \gg 1/\tau$), the negative-compliance element, which has value $-c_{12}\,c_{21}/C_{\mathrm{m}}$, where $C_{\mathrm{m}} = G_K\,\tau$, dominates instead and the resistive element becomes negligible. Since CF $\gg 1/\tau$ at almost all locations in the cochlea, we are interested in the high-frequency condition, where the main effect of the mechanical-to-electrical coupling is to add to the passive OHC compliance a negative compliance, resulting in a stiffer OHC and a smaller $Y_{\mathrm{ohc,eff}}$. Since $Y_{\mathrm{ohc,eff}}$ decreases, the magnitude of the active force generator F_{ohc} increases. Note that for $c_{12} = 0$, the case considered in the main text, the active force generator in Fig. 19 reduces to the original force generator described in Eq. (2). The new effective OHC voltage-to-force gain, $k_{\mathrm{f,eff}}$, is given by $s \times c_{21}/Y_{\mathrm{ohc,eff}}$. Substituting in the effective OHC gain $k_{\mathrm{f,eff}}$ for k_{f} and $Y_{\mathrm{ohc,eff}}$ for Y_{ohc} in the loop gain from Eq. (6) yields the new loop gain:

$$\frac{c_{21}k_{\mathrm{v}}}{(\tau s+1)}\,\frac{Y_{\mathrm{rl}}}{Y_{\mathrm{bm}}+Y_{\mathrm{rl}}+Y_{\mathrm{ohc,eff}}} \tag{13}$$

According to Eq. (13), the mechanical-to-electrical coupling increases the net OHC stiffness, which reduces the OHC mechanical admittance, $Y_{\mathrm{ohc,eff}}$, and thus increases the loop gain. Eq. (13) also describes how OHC damage or other mechanisms described above may lower the loop gain and increase the sensitivity of low-frequency tuning-curve tails – either by reducing the piezoelectric coefficient or by reducing the OHC stiffness. These mechanisms are not mutually exclusive.

Assuming $c_{12} = c_{21} = 20$ fC/nN (Dong et al., 2002) and $C_{\mathrm{m}} = 13$ pF at the basal end, the negative compliance from the mechanical-to-electrical coupling is -30.77 m/N, which is on the same order of magnitude as the passive OHC compliance, $C_{\mathrm{ohc}} = 39.3$ m/N. Clearly, the piezoelectric mechanical-to-electrical coupling can significantly increase the OHC stiffness, which is advantageous because it increases the efficiency of the negative-feedback loop and helps to speedup the slow OHCs. Thus, the piezoelectric coupling acts as a minor negative-feedback loop that helps increase the gain of the major negative-feedback loop described in the main text. By increasing the loop gain, piezoelectricity helps extend the OHC bandwidth. The use of major and minor feedback loops in this fashion is commonplace in engineering, e.g. minor tachometer feedback loops are often embedded in major Proportional Integral-Derivative (PID) control loops for motor control (Franklin et al., 2002).

4. Discussion

Our model does not require novel mechanisms that have not been observed and simply simulates cochlear functional anatomy. Our parameters were derived from experimental literature. We assumed a maximum k_{f} of 0.5 nN/mV in the basal end, which lies between 0.5 nN/mV and 1.25 nN/mV, the estimated upper limits for the OHC force gains (Mountain and Hubbard, 1994; Iwasa and Chadwick, 1992). To demonstrate that our model could yield significant speed-ups, we purposely chose membrane time constants that were on the slow end of measured data. Guinea pig OHCs with a minimum $\tau = 0.15$ ms at the base and a maximum of 3 ms at the apex have been measured (Housley and Ashmore, 1992; Preyer et al., 1996), compared to the respective minimum, 0.3 ms, and maximum, 9.4 ms, used in our model. Had we adopted faster but still realistic time constants, we could have decreased the maximum k_{f} required by over a factor of two to three, as shown in Fig. 15. Furthermore, we assumed quality factors for the RL that were conservative compared with estimates of the TM-RL gap damping (Eq. (7)) though perhaps not compared to recent data (Scherer and Gummer, 2004a). By modifying other passive parameters within the limits of experimental evidence (Fig. 16), we can reduce the necessary OHC gain further. Nonetheless, we chose to use the upper limit of k_{f} to demonstrate how far the system can be pushed. Thus, OHCs have adequate gain for mechanical amplification despite slow membrane RC time constants.

Past multiple-mode models that have successfully matched data have also implicitly used negative feedback, although they did not incorporate OHCs with slow membrane time constants and thus did not realize the importance of negative feedback on reducing the time-constant limitation (Hubbard et al., 2000; Hubbard, 1993). Negative feedback around the BM has been proposed in previous work (Mountain et al., 1983; Khanna and Hao, 2000). However, in our model, it is negative feedback around the RL and not the BM that is important for fast amplification with slow OHCs. Since basal OHCs contract due to depolarization as a result of upwards RL or BM movement, thus pulling the RL down and the BM up, negative feedback is around the RL and not the BM. We have used engineering concepts to analyze experimental data in the high-frequency region, as previously attempted (Zweig, 1991), in order to gain insight into the operation of this biological system (Csete and Doyle, 2002).

Others have incorporated OHCs with the membrane time constant into their models but have not described how the OHC time constant limitation was overcome (Geisler and Sang, 1995; Fukazawa, 1997; Neely, 1993; Dimitriadis and Chadwick, 1999). For example, Dimitriadis and Chadwick (1999) describe a two-oscillator model that requires only 20 pN/cell to produce amplification with the OHC membrane time constant. We have attempted to explain how amplification with time constant limitation is possible rather than claim to be the first to model a system with the RC time constant.

Scherer and Gummer (2004a) have recently shown that the organ of Corti is viscoelastic and has a viscous component that is twice the stiffness component at CF in the basal region. These results suggest that there may be a mechanical zero located at a frequency equal to CF/2 based on a model by Nobili and Mammano (1996). According to this model, the mechanical zero compensates for the OHC time

constant. Our model is not mutually exclusive with Scherer and Gummer's (2004a) observations and Nobili and Mammano's theory (1996). As described above in Section 3, negative feedback moves the closed-loop OHC pole to 7.46 kHz, which is still a factor of 5.8 from CF at the basal end. Thus, there is still an attenuation of the OHC force in our model. The presence of a mechanical zero at CF/2 could help compensate for the residual attenuation. Furthermore, Scherer and Gummer (2004a) calculated the required ratio for viscous to elastic force at CF to be 33 based on the Nobili and Mammano (1996) model but found that the ratio was only two experimentally, suggesting that the mechanical zero is at a much higher frequency than the inherent OHC time constant. If there was no OHC speedup due to negative feedback, there would still be a significant drop in the OHC force in the frequency range between the open-loop OHC pole and the mechanical zero. However, with negative feedback in our model, the closed-loop OHC pole is moved to a higher frequency and could be more readily compensated for by the mechanical zero.

Recent results by Scherer and Gummer (2004b) have also demonstrated that the in vitro OHC force response without a TM and with a clamped BM exhibits a broad resonance near CF at the base of the cochlea. This resonance may help to compensate for reduction of the membrane potential due to the membrane time constant but is probably inadequate to provide full compensation since it has a maximum peak that is less than 10 dB and has a relatively constant phase up to CF (Scherer and Gummer, 2004b). Thus, the resonance may be more important in counteracting the viscoelastic organ of Corti rather than the membrane time constant, which can be readily compensated for by negative feedback even without the OHC force resonance, as we have demonstrated. The OHC forces measured in this in vitro preparation (50–300 pN/mV) are in the range of values of k_f used in our model (Scherer and Gummer, 2004b). Future iterations of our model that include these newly described characteristics of the OHC force response will help elucidate the effect of the broad OHC force resonance and organ-of-Corti viscoelasticity on OHC mechanics.

Finally, our theory for cochlear amplification with negative feedback is not restricted to a two-resonator model of cochlear micromechanics. Three root locus plots are shown in Fig. 20 – the first is for our micromechanical model without RL mass (Fig. 20a), the second is for a model without BM mass (Fig. 20b), and the third is for a model without RL or BM mass (Fig. 20c). Thus, the first and second models have only one passive resonator and the third model has no passive resonators. Fig. 20a shows that increasing OHC gain will speed up the slow OHC membrane time constant on the real axis. In fact, at high OHC gains, the two poles on the real axis collide and become complex, creating a resonant pair of poles. However, these poles do not move directly towards the imaginary axis but move more parallel to it; thus, they do not increase their resonant gain as effectively as in

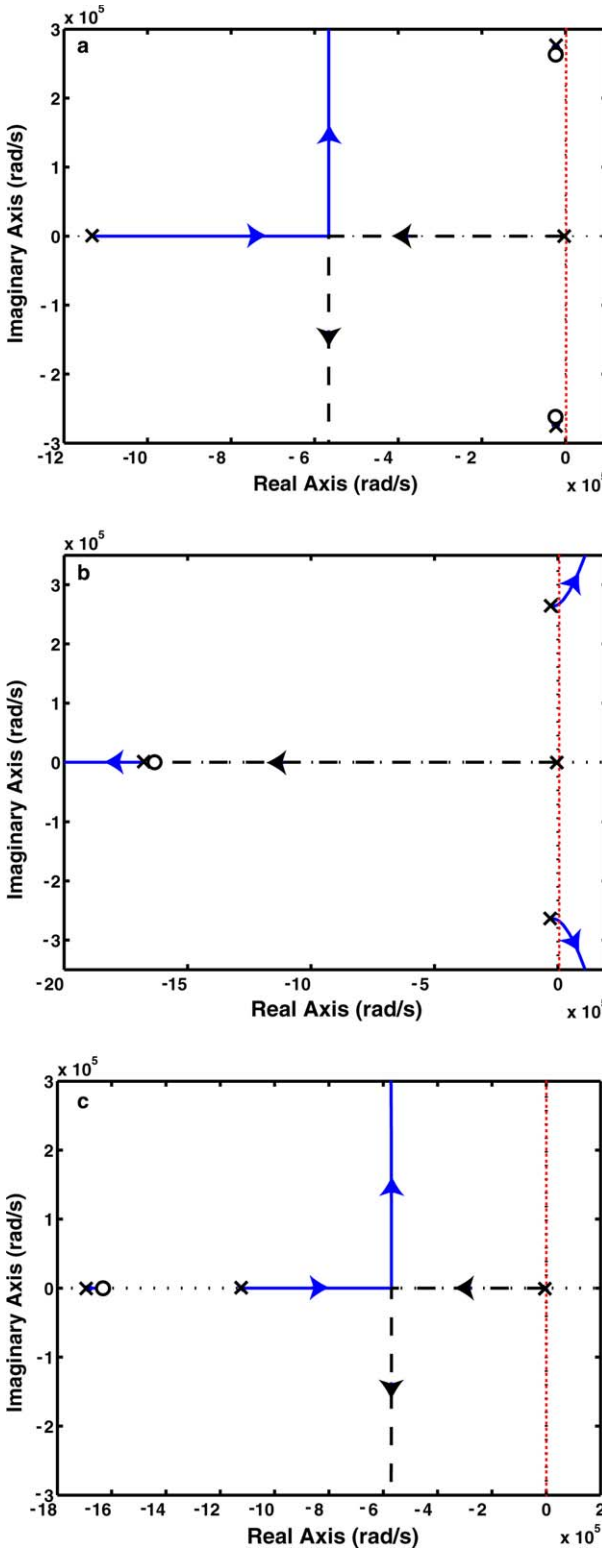

Fig. 20. Root locus plots for (a) no TM-RL mass, (b) no BM mass, and (c) no TM-RL or BM masses. In all three cases, the slow OHC time constant represented by the pole near the origin moves away from the origin with increasing gain. However, only when the model has TM-RL mass (as in case (b)) does a pair of poles move towards the imaginary axis to effectively increase resonant gain. Therefore, although negative feedback can still speedup the slow OHC membrane time constant when TM-RL or BM masses can be negligible, a resonant TM-RL increases the effectiveness of the feedback loop in increasing resonant gain.

our prior model. There is a complex pair of poles in Fig. 20a as well, but these do not move far due to nearby zeros. In contrast, Fig. 20b shows that increasing OHC gain will not only speed up the slow OHC membrane time constant on the real axis, but it will also increase the resonant gain of the complex poles. Finally, Fig. 20c shows that without any passive resonators, the slow membrane time constant can still be sped up to the point where the two real poles collide and create complex poles. Thus, even in a system without any passive resonators, resonant behavior can be created by the movement of singularities caused by negative feedback. However, as with Fig. 20a, these poles travel parallel to the imaginary axis and thus do not increase resonant gain as effectively as in our prior model. Therefore, although a two-resonator model of cochlear micromechanics as we presented earlier is not necessary for speedup of the slow membrane time constant with negative feedback, it assists in producing cochlear amplification by making the increase in resonant gain more effective.

We believe that our general theory for speedup will be invariant with detailed parameter choices in our model or other more complex cochlear models. However, our model clearly has limitations that need to be addressed in future work. For example, our phase data in Fig. 12b rolls off faster than experimental data (Ruggero et al., 1990). Also, we tapered our k_f such that the peak magnitude response falls more steeply from the 10 kHz location to the 1 kHz location in the cochlea (Fig. 14a) than seen in most auditory nerve responses. Our fit to data could be improved by simply decreasing the steepness of our k_f taper, which would result in higher peak magnitudes in the more apical regions of the cochlea; as described in Section 2.3.2, our *kf* taper was determined somewhat arbitrarily due to the lack of in vivo data. Additionally, we tapered our RL stiffness significantly more than is found in some experimental data (Scherer and Gummer, 2004a); we used a constant RL damping instead of a frequency-dependent one (Scherer and Gummer, 2004a); and some recent experiments have suggested that the damping at the RL could actually be an order of magnitude higher than we have assumed (Scherer and Gummer, 2004a). These issues do not change our basic ideas for speedup but suggest that our OHC gain-bandwidth product may need to be higher to attain the required amplification and/or a higher-order coupled-resonator model of the TM–RL complex may be necessary such that more gain is available at one local stage of the cochlea. We also used parameters from a variety of species although the ideal situation would be to have parameters and experimental data from the same species.

5. Conclusions

Our model is clearly a simplification of complex cochlear mechanics. Given that we derived our parameters and experimental data from a variety of individual animals, species, and laboratories, the model we have presented here is not meant to be a definitive one that fits all data. Although others have incorporated the OHC time constant into their models, they have not explained how the OHC time constant limitation was overcome (Geisler and Sang, 1995; Fukazawa, 1997; Neely, 1993; Dimitriadis and Chadwick, 1999). Our key contribution is demonstrating that a reasonable cochlear model incorporating negative feedback with a sufficient gain-bandwidth product can provide speedup in the overall closed-loop system. In such closed-loop systems, it is the gain-bandwidth product that matters, not just the bandwidth. To present the essential insights necessary to understand fast cochlear amplification with slow OHCs, we focused on organ-of-Corti dynamics with numerous simplifications, such as a 1D fluid approximation. Our model may be further extended to capture more detailed phenomena. The addition of nonlinearities, active OHC stiffness, higher-order micromechanical, macromechanical, and fluid dimensionality (Kolston, 1999; Lim and Steele, 2002; Steele, 1999), time-domain simulations, and other complexities will not alter the fundamental insights described here.

These insights we described are: (1) Feedback in the cochlea is negative at DC because the corrective action of the OHC-RL subsystem opposes changes to the output caused by changes in the input. The less stiff RL compared with the BM maximizes the negative feedback. (2) The OHC gain-bandwidth product is sufficient to provide fast cochlear amplification in a negative-feedback closed-loop system with reasonable measured parameters for OHC gain and bandwidth. (3) Our model fits experimental data with reasonable parameters. (4) The speedup or gain increase due to negative feedback does not need to be large at any local OHC stage because of the cochlea's collective traveling-wave action. (5) Piezoelectric effects increase the effectiveness of the negative-feedback loop to yield higher loop gain and more OHC speedup but are not required for high-frequency amplification in our model.

Acknowledgements

We are grateful for useful suggestions and feedback from W. E. Brownell. We would like to thank M. Ruggero for granting us permission to use his experimental data. T.K.L is a Howard Hughes Medical Institute Predoctoral Fellow. This work is also supported in part by a CAREER award from the National Science Foundation, a Packard award, and an ONR Young Investigator award.

References

Allen, J.B., 1980. Cochlear micromechanics – a physical model of transduction. J. Acoust. Soc. Am. 68, 1660–1670.

Bode, H.W., 1945. Network Analysis and Feedback Amplifier Design. D. van Nostrand, Princeton, NJ.

Brownell, W.E., Bader, C.R., Bertrand, D., Ribaupierre, Y., 1985. Evoked mechanical responses of isolated cochlear outer hair cells. Science 227, 194–196.

Chadwick, R.S., Dimitriadis, E.K., Iwasa, K.H., 1996. Active control of waves in a cochlear model with subpartitions. Proc. Natl. Acad. Sci. U.S.A. 93, 2564–2569.

Chan, D.K., Hudspeth, A.J., 2005. Ca^{2+} current-driven nonlinear amplification by the mammalian cochlea in vitro. Nat. Neurosci. 8, 149–155.

Cheatham, M.A., Huynh, K.H., Gao, J., Zuo, J., Dallos, P., 2004. Cochlear function in Prestin knockout mice. J. Physiol. 560, 821–830.

Choe, Y., Magnasco, M.O., Husdpeth, A.J., 1998. A model for amplification of hair-bundle motion by cyclical binding of Ca^{2+} to mechanoelectrical-transduction channels. Proc. Natl. Acad. Sci. U.S.A. 95, 15321–15326.

Cody, A.R., 1992. Acoustic lesions in the mammalian cochlea – implications for the spatial-distribution of the active process. Hear. Res. 62, 166–172.

Cooper, N.P., Rhode, W.S., 1992. Basilar membrane mechanics in the hook region of the cat and guinea-pig cochlea: sharp tuning and nonlinearity in the absence of baseline position shifts. Hear. Res. 63, 163–190.

Csete, M.E., Doyle, J.C., 2002. Reverse engineering of biological complexity. Science 295, 1664–1669.

Dallos, P., Evans, B.N., 1995. High-frequency motility of outer hair cells and the cochlear amplifier. Science 267, 2006–2009.

de Boer, E., 1990a. Wave-propagation modes and boundary conditions for the Ulfendahl-Flock-Khanna (UFK) preparation. In: Dallos, P., Geisler, C.D., Matthews, J.W., Ruggero, M.A., Steele, C.R. (Eds.), Mechanics and Biophysics of Hearing. Spring-Verlag, Berlin, pp. 333–339.

de Boer, E., 1990b. Can shape deformations of the organ of Corti influence the travelling wave in the cochlea? Hear. Res. 44, 83–92.

de Boer, E., Nuttall, A.L., 2000. The mechanical waveform of the basilar membrane. III. Intensity effects. J. Acoust. Soc. Am. 107, 1497–1507.

Deen, W.M., 1998. Analysis of Transport Phenomena. Oxford Univ. Press, New York, pp. 253–254.

Deo, N., Grosh, K., 2004. Two-state model for outer hair cell stiffness and motility. Biophys. J. 86, 3519–3528.

Dimitriadis, E.K., Chadwick, R.S., 1999. Solution of the inverse problem for a linear cochlear model: A tonotopic cochlear amplifier. J. Acoust. Soc. Am. 106, 1880–1892.

Dong, X.X., Ospeck, M., Iwasa, K.H., 2002. Piezoelectric reciprocal relationship of the membrane motor in the cochlear outer hair cell. Biophys. J. 82, 1254–1259.

Emadi, G., Richter, C.P., Dallos, P., 2004. Stiffness of the gerbil basilar membrane: radial and longitudinal variations. J. Neurophysiol. 91, 474–488.

Fernández, C., 1952. Dimensions of the Cochlea (Guinea Pig). J. Acoust. Soc. Am. 24, 519–523.

Fitzgerald, J.J., Robertson, D., Johnstone, B.M., 1993. Effects of intracochlear perfusion of salicylates on cochlear microphonic and other auditory responses in the guinea pig. Hear. Res. 67, 147–156.

Frank, G., Hemmert, W., Gummer, A.W., 1999. Limiting dynamics of high-frequency electromechanical transduction of outer hair cells. Proc. Natl. Acad. Sci. U.S.A. 96, 4420–4425.

Franklin, G.F., Powell, J.D., Emami-Naeini, A., 2002. Feedback Control of Dynamic Systems, fourth ed. Prentice Hall, New Jersey.

Freeman, D.M., Weiss, T.F., 1990a. Hydrodynamic forces on hair bundles at low frequencies. Hear. Res. 48, 17–30.

Freeman, D.M., Weiss, T.F., 1990b. Hydrodynamic forces on hair bundles at high frequencies. Hear. Res. 48, 31–36.

Fukazawa, T., 1997. A model of cochlear micromechanics. Hear. Res. 113, 182–190.

Geisler, C.D., Sang, C., 1995. A cochlear model using feed-forward outer hair cell forces. Hear. Res. 86, 132–146.

Greenwood, D.D., 1990. A cochlear frequency-position function for several species–29 years later. J. Acoust. Soc. Am. 87, 2592–2605.

Guinan Jr., J.J., Gifford, M.L., 1988. Effects of electrical stimulation of efferent olivocochlear neurons on cat auditory-nerve fibers. III. Tuning curves and thresholds at CF.. Hear. Res. 37, 29–45.

Gummer, A.W., Hemmert, W., Zenner, H.P., 1996. Resonant tectorial membrane motion in the inner ear: its crucial role in frequency tuning. Proc. Natl. Acad. Sci. U.S.A. 93, 8727–8732.

He, D.Z., Dallos, P., 1999. Somatic stiffness of cochlear outer hair cells is voltage-dependent. Proc. Natl. Acad. Sci. U.S.A. 96, 8223–8228.

He, D.Z., Jia, S., Dallos, P., 2004. Mechanoelectrical transduction of adult outer hair cells studied in a gerbil hemicochlea. Nature 429, 766–770.

Housley, G.D., Ashmore, J.F., 1992. Ionic currents of outer hair cells isolated from the guinea-pig cochlea. J. Physiol. 448, 73–98.

Hubbard, A.E., 1993. A traveling-wave amplifier model of the cochlea. Science 259, 68–71.

Hubbard, A.E., Yang, Z., Shatz, L., Mountain, DC, 2000. Multi-mode cochlear models. In: Wada, H., Takasaka, T., Ikeda, K., Ohyama, K., Koike, T. (Eds.), Symposium on Recent Developments in Auditory Mechanics. World Scientific Publishing, Singapore, pp. 167–173.

Iwasa, K.H., Chadwick, R.S., 1992. Elasticity and active force generation of cochlear outer hair cells. J. Acoust. Soc. Am. 92, 3169–3173.

Kennedy, H.J., Crawford, A.C., Fettiplace, R., 2005. Force generation by mammalian hair bundles supports a role in cochlear amplification. Nature 433, 880–883.

Khanna, S.M., Hao, L.F., 2000. Amplification in the apical turn of the cochlea with negative feedback. Hear. Res. 149, 55–76.

Kinsler, L.E., Frey, A.R., 1962. Fundamentals of Acoustics, second ed. Wiley, New York, pp. 186–193.

Kolston, P.J., 1999. Comparing in vitro, in situ, and in vivo experimental data in a three-dimensional model of mammalian cochlear mechanics. Proc. Natl. Acad. Sci. U.S.A. 96, 3676–3681.

Liberman, M.C., Dodds, L.W., 1984. Single-neuron labeling and chronic cochlear pathology. III. Stereocilia damage and alterations of threshold tuning curves. Hear. Res. 16, 55–74.

Liberman, M.C., Gao, J., He, D.Z., Wu, X., Jia, S., Zuo, J., 2002. Prestin is required for electromotility of the outer hair cell and for the cochlear amplifier. Nature 419, 300–304.

Lim, K.M., Steele, C.R., 2002. A three-dimensional nonlinear active cochlear model analyzed by the WKB-numeric method. Hear. Res. 170, 190–205.

Lu, T.K., 2003. A Feedback Analysis of Outer Hair Cell Dynamics. M.Eng. Thesis, Massachusetts Institute of Technology, Massachusetts. 146pp.

Lu, T.K., Zhak, S., Dallos, P., Sarpeshkar, R., 2006. A micromechanical model for fast cochlear amplification with slow outer hair cells. In: Nuttall, A.L., Gillespie, P., Ren, T., Grosh, K., de Boer, E. (Eds.), Auditory Mechanisms: Processes and Models. World Scientific Publishing, Singapore, pp. 432–440.

Lynch III, T.J., Nedzelnitsky, V., Peake, W.T., 1982. Input impedance of the cochlea in cat. J. Acoust. Soc. Am. 72, 108–130.

Mammano, F., Ashmore, J.F., 1993. Reverse transduction measured in the isolated cochlea by laser Michelson interferometry. Nature 365, 838–841.

Markin, V.S., Hudspeth, A.J., 1995. Modeling the active process of the cochlea: phase relations, amplification, and spontaneous oscillation. Biophys. J. 69, 138–174.

Mountain, DC, Hubbard, A.E., 1994. A piezoelectric model of outer hair cell function. J. Acoust. Soc. Am. 95, 350–354.

Mountain, DC, Karavitaki, K.D., 2003. Presented at the 146th Meeting of the Acoustical Society of America, Austin, TX, [online] (13 Nov. 2003). Available from: <http://www.acoustics.org/press/146th/mountain.htm>.

Mountain, DC, Hubbard, A.E., McMullen, T.A., 1983. Electromechanical processes in the cochlea. In: de Boer, E., Viergever, M.A. (Eds.), Mechanics of Hearing. Delft University Press, The Netherlands, pp. 119–126.

Murugasu, E., Russell, I.J., 1996. The effect of efferent stimulation on basilar membrane displacement in the basal turn of the guinea pig cochlea. J. Neurosci. 16, 325–332.

Naidu, R.C., Mountain, DC, 1998. Measurements of the stiffness map challenge a basic tenet of cochlear theories. Hear. Res. 124, 124–131.

Neely, S.T., 1993. A model of cochlear mechanics with outer hair cell motility. J. Acoust. Soc. Am. 94, 137–146.
Neely, S.T., Kim, D.O., 1986. A model for active elements in cochlear biomechanics. J. Acoust. Soc. Am. 79, 1472–1480.
Nilsen, K.E., Russell, I.J., 2000. The spatial and temporal representation of a tone on the guinea pig basilar membrane. Proc. Natl. Acad. Sci. U.S.A. 97, 11751–11758.
Nobili, R., Mammano, F., 1996. Biophysics of the cochlea. II: Stationary nonlinear phenomenology. J. Acoust. Soc. Am. 99, 2244–2255.
Ospeck, M., Dong, X.X., Iwasa, K.H., 2003. Limiting frequency of the cochlear amplifier based on electromotility of outer hair cells. Biophys. J. 84, 739–749.
Overstreet, E.H., Temchin, A.N., Ruggero, M.A., 2002. Passive basilar membrane vibrations in gerbil neonates: mechanical bases of cochlear maturation. J. Physiol. 545, 279–288.
Preyer, S., Hemmert, W., Pfister, M., Zenner, H.P., Gummer, A.W., 1994. Frequency response of mature guinea-pig outer hair cells to stereociliary displacement. Hear. Res. 77, 116–124.
Preyer, S., Renz, S., Hemmert, W., Zenner, H.P., Gummer, A.W., 1996. Receptor potential of outer hair cells isolated from base to apex of the adult guinea-pig cochlea: Implications for cochlear tuning mechanisms. Aud. Neurosci. 2, 145–157.
Puria, S., Allen, J.B., 1991. A parametric study of cochlear input impedance. J. Acoust. Soc. Am. 89, 287–309.
Ren, T., Nuttall, A.L., 2001. Basilar membrane vibration in the basal turn of the sensitive gerbil cochlea. Hear. Res. 151, 48–60.
Reuter, G., Zenner, H.P., 1990. Active radial and transverse motile responses of outer hair cells in the organ of Corti. Hear. Res. 43, 219–230.
Robles, L., Ruggero, M.A., 2001. Mechanics of the mammalian cochlea. Physiol. Rev. 81, 1305–1352.
Ruggero, M.A., Rich, N.C., Robles, L., Shivapuja, B.G., 1990. Middle-ear response in the chinchilla and its relationship to mechanics at the base of the cochlea. J. Acoust. Soc. Am. 87, 1612–1629.
Santos-Sacchi, J., 2003. New tunes from Corti's organ: the outer hair cell boogie rules. Curr. Opin. Neurobiol. 13, 459–468.
Sarpeshkar, R., 2000. Traveling waves versus bandpass filters: the silicon and biological cochlea. In: Wada, H., Takasaka, T., Ikeda, K., Ohyama, K., Koike, T. (Eds.), Symposium on Recent Developments in Auditory Mechanics. World Scientific Publishing, Singapore, pp. 216–222.
Sarpeshkar, R., Lyon, R.F., Mead, C.A., 1998. A low-power wide-dynamic-range analog VLSI cochlea. Analog Integrated Circuits and Signal Processing 16, 245–274.
Scherer, M.P., Gummer, A.W., 2004a. Impedance analysis of the organ of Corti with magnetically actuated probes. Biophys. J. 87, 1378–1391.
Scherer, M.P., Gummer, A.W., 2004b. Vibration pattern of the organ of Corti up to 50 kHz: Evidence for resonant electromechanical force. Proc. Natl. Acad. Sci. U.S.A. 101, 17652–17657.
Sellick, P.M., Yates, G.K., Patuzzi, R., 1983. The influence of Mössbauer source size and position on phase and amplitude measurements of the guinea pig basilar membrane. Hear. Res. 10, 101–108.
Shera, C.A., 2003. Mammalian spontaneous otoacoustic emissions are amplitude-stabilized cochlear standing waves. J. Acoust. Soc. Am. 114, 244–262.
Shera, C.A., Zweig, G., 1991. A symmetry suppresses the cochlear catastrophe. J. Acoust. Soc. Am. 89, 1276–1289.
Spector, A.A., 2005. Effectiveness, active energy produced by molecular motors, and nonlinear capacitance of the cochlear outer hair cell. J. Biomech. Eng. 127, 391–399.
Spector, A.A., Brownell, W.E., Popel, A.S., 2003. Effect of outer hair cell piezoelectricity on high-frequency receptor potentials. J. Acoust. Soc. Am. 113, 453–461.
Spector, A.A., Popel, A.S., Eatock, R.A., Brownell, W.E., 2005. Mechanosensitive channels in the lateral wall can enhance the cochlear outer hair cell frequency response. Ann. Biomed. Eng. 33, 991–1002.
Steele, C.R., 1999. Toward three-dimensional analysis of cochlear structure. ORL J. Otorhinolaryngol. Relat. Spec. 61, 238–251.
Stenfelt, S., Hato, N., Goode, R.L., 2004. Fluid volume displacement at the oval and round windows with air and bone conduction stimulation. J. Acoust. Soc. Am. 115, 797–812.
Talmadge, C.L., Tubis, A., Long, G.R., Piskorski, P., 1998. Modeling otoacoustic emission and hearing threshold fine structures. J. Acoust. Soc. Am. 104, 1517–1543.
Thorne, P.R., Gavin, J.B., 1984. The accuracy of hair cell counts in determining distance and position along the organ of Corti. J. Acoust. Soc. Am. 76, 440–442.
Thorne, M., Salt, A.N., DeMott, J.E., Henson, M.M., Henson Jr., O.W., Gewalt, S.L., 1999. Cochlear fluid space dimensions for six species derived from reconstructions of three-dimensional magnetic resonance images. Laryngoscope 109, 1661–1668.
Ulfendahl, M., Khanna, S.M., Heneghan, C., 1995. Shearing motion in the hearing organ measured by confocal laser heterodyne interferometry. Neuroreport 6, 1157–1160.
von Békésy, G., 1960. Experiments in Hearing. McGraw-Hill, New York, pp. 406.
Weitzel, E.K., Tasker, R., Brownell, W.E., 2003. Outer hair cell piezoelectricity: frequency response enhancement and resonance behavior. J. Acoust. Soc. Am. 114, 1462–1466.
Wilson, J.P., Johnstone, J.R., 1975. Basilar membrane and middle-ear vibration in guinea pig measured by capacitive probe. Hear. Res. 57, 705–723.
Wright, A., 1984. Dimensions of the cochlear stereocilia in man and the guinea pig. Hear. Res. 13, 89–94.
Zweig, G., 1991. Finding the impedance of the organ of Corti. J. Acoust. Soc. Am. 89, 1229–1254.
Zweig, G., Shera, C.A., 1995. The origin of periodicity in the spectrum of evoked otoacoustic emissions. J. Acoust. Soc. Am. 98, 2018–2047.
Zwislocki, J.J., 1979. Tectorial membrane: a possible sharpening effect on the frequency analysis in the cochlea. Acta Otolaryngol. 87, 267–269.
Zwislocki, J.J., Kletsky, E.J., 1979. Tectorial membrane: a possible effect on frequency analysis in the cochlear. Science 204, 639–641.